

**OPTIMIZATION OF THE BOTTOM PROFILE OF U-SHAPE
OSCILLATING WATER COLUMN**

TAY CHIH CHIA

**A project report submitted in partial fulfilment of the
requirements for the award of Bachelor of Engineering
(Honours) Mechanical Engineering**

**Lee Kong Chian Faculty of Engineering and Science
Universiti Tunku Abdul Rahman**

April 2019

DECLARATION

I hereby declare that this project report is based on my original work except for citations and quotations which have been duly acknowledged. I also declare that it has not been previously and concurrently submitted for any other degree or award at UTAR or other institutions.

Signature : _____

Name : Tay Chih Chia

ID No. : 14UEB02364

Date : _____

APPROVAL FOR SUBMISSION

I certify that this project report entitled “**OPTIMIZATION OF THE BOTTOM PROFILE OF U-SHAPE OSCILLATING WATER COLUMN**” was prepared by **TAY CHIH CHIA** has met the required standard for submission in partial fulfilment of the requirements for the award of Bachelor of Engineering (Honours) Mechanical Engineering at Universiti Tunku Abdul Rahman.

Approved by,

Signature : _____

Supervisor : Ts. Dr. Jun Hieng Kiat

Date : _____

Signature : _____

Co-Supervisor : _____

Date : _____

The copyright of this report belongs to the author under the terms of the copyright Act 1987 as qualified by Intellectual Property Policy of Universiti Tunku Abdul Rahman. Due acknowledgement shall always be made of the use of any material contained in, or derived from, this report.

© 2019, Tay Chih Chia. All right reserved.

ACKNOWLEDGEMENTS

I wish to express my sincere gratitude to my research supervisor, Ts. Dr. Jun Hieng Kiat for his valuable guidance, suggestion and his enormous patience throughout the development of the research.

I would like to thank my senior, Mr. Tan Chang Ting, who had provided help, support and valuable hints during the simulation process of ANSYS Computational Fluid Dynamics.

Furthermore, I would like to express my sincere appreciation to my housemate, Mr. Wong Wee Ken for the abundant support and guidance throughout the construction of the Arduino water wave generator.

Finally, I would also like to acknowledge with gratitude, the warmest support and love from my parents and my brothers, who had helped and given me encouragement throughout the research development.

ABSTRACT

U-Shape Oscillating Water Column (U-OWC) is found to have better efficiency than the conventional Oscillating Water Column (OWC). Although the overall shape of the OWC has been popularly researched in the field of wave energy, the studies on internal structure of the OWC is considerably lacking. The aim of this study was to determine the optimum bottom profile for the U-OWC structure that can deliver the best performance of U-OWC. ANSYS CFX simulation was performed on four U-OWC models with different bottom profile namely, flat, circular, 1:1 slope and 1:5 slope. The simulation results confirmed that the circular bottom profile has the greatest configuration to yield the highest air-discharge velocity, and power output. This was followed by 1:1 slope bottom profile, 1:5 slope bottom profile and flat bottom profile. Based on the simulated circular bottom profile U-OWC structure, prototype was fabricated to verify the simulation results. The percentage error between the simulated power output and the experimental power output was determined. Factors that were accounted for the error contribution were discussed. In overall, the identification of circular shape as the optimum design for the U-OWC bottom profile may help to increase the power efficiency of the future OWC structures as well as to provide supporting information for the future research projects on the parametric optimization of U-OWC.

TABLE OF CONTENTS

DECLARATION	ii
APPROVAL FOR SUBMISSION	iii
ACKNOWLEDGEMENTS	v
ABSTRACT	vi
TABLE OF CONTENTS	vii
LIST OF TABLES	xi
LIST OF FIGURES	xii
LIST OF SYMBOLS / ABBREVIATIONS	xviii
LIST OF APPENDICES	xix

CHAPTER

1	INTRODUCTION	1
	1.1 General Introduction	1
	1.1.1 Wave Energy Potential in Malaysia	1
	1.1.2 Oscillating Water Column	2
	1.2 Importance of the Study	3
	1.3 Problem Statement	4
	1.4 Aim and Objectives	4
	1.5 Scope and Limitation of the Study	4
	1.6 Contribution of the Study	5
	1.7 Outline of the Report	5
2	LITERATURE REVIEW	6
	2.1 Introduction	6
	2.2 Operation of OWC	6
	2.3 Performances of OWC with Different Shapes	7
	2.3.1 Comparison of U-OWC and Conventional OWCs	7

2.3.2	Effects of Incline Orientation on OWC	9
2.3.3	Wave Collector	10
2.4	Parametric Optimization of OWC	11
2.4.1	Chamber Front Wall Orientation	11
2.4.2	Chamber Front Wall Immersion Depth	12
2.4.3	Chamber Inner Bottom Profile	12
2.4.4	Chamber Length	13
2.4.5	Orifice Dimension	14
2.5	Power Conversion of OWC	14
2.5.1	Incompressible Air	17
2.5.2	Ideal Air	18
2.6	ANSYS Computational Fluid Dynamics	18
2.7	Summary	19
3	METHODOLOGY AND WORK PLAN	20
3.1	Introduction	20
3.2	Work Plan	21
3.3	Design Phase	22
3.3.1	Optimum Dimensions of U-OWC	22
3.3.2	Dimensions of the Different Bottom Profiles	23
3.4	Simulation Phase	25
3.4.1	3D Modeling	26
3.4.2	Meshing	31
3.4.3	Setup	32
3.4.4	Solution Generation	39
3.4.5	CFD-Post	40
3.5	Experimental Phase	46
3.5.1	Water Tank	47
3.5.2	U-OWC Chamber with Circular Bottom Profile	47
3.5.3	Enhancement Frames for Water Tank Walls	48
3.5.4	Arduino Water Wave Generator	49
3.5.5	Arduino Pressure Sensor	52
3.5.6	Experiment Setup	53

4	RESULTS AND DISCUSSIONS	55
4.1	Introduction	55
4.2	Simulation Results	55
4.2.1	Flat Bottom Profile U-OWC	55
4.2.2	Slope 1:1 Bottom Profile U-OWC	56
4.2.3	Slope 1: 5 Bottom Profile U-OWC	58
4.2.4	Circular Bottom Profile U-OWC	59
4.2.5	Data Extraction from the Steady-State Time Steps	60
4.2.6	Comparison of Simulation Results of the Four U-OWC Models	60
4.2.7	Selection of the Optimum Bottom Profile of U-OWC	61
4.3	Experimental Results	62
4.3.1	Comparison of Average Velocity and Average Pressure between Optimum Simulated U-OWC and Experimental U-OWC	63
4.3.2	Comparison of Power Output between Optimum Simulated U-OWC and Experimental U-OWC	64
4.4	Causes of the Percentage Error	65
4.4.1	Simulation Error	65
4.4.2	Experimental Errors	66
5	CONCLUSIONS AND RECOMMENDATIONS	68
5.1	Conclusions	68
5.2	Problems Encountered in the Simulation Phase	69
5.2.1	Lengthy Time of Simulation Phase	69
5.2.2	Simulation Failure due to “Isolated Fluid Region” Error	69
5.2.3	Simulation Failure due to “Overflow in Linear Solver” Error	69
5.3	Problems Encountered in the Experimental Phase	70
5.3.1	Leaking Water Tank	70

5.3.2	Mechanical Failure of the Arm-linkages of the Servo Motors	70
5.3.3	Synchronization of the Paddles Motions of the Arduino Water Wave Generator	71
5.4	Limitations of the Project	71
5.5	Recommendations for the Future Project	72
	REFERENCES	73
	APPENDICES	76

LIST OF TABLES

Table 1.1:	Wave Data from Potential Locations in Malaysia (Samrat et al., 2014)	2
Table 3.1:	Dimensions of Optimum U-OWC with multiplication factor of 0.04	23
Table 3.2:	Number of Nodes and Elements for the Four U-OWC 3D Models	32
Table 4.1:	Summary of the Simulation Results	62

LIST OF FIGURES

Figure 1.1:	Schematic Diagram of an Offshore OWC (Falcão and Henriques, 2016)	3
Figure 1.2:	Schematic Diagram of an Onshore OWC (Falcão and Henriques, 2016)	3
Figure 2.1:	Mechanisms of an Onshore Fixed OWC (Office of Energy Efficiency & Renewable Energy, 2018)	7
Figure 2.2:	Schematic Diagram of OWCs	8
Figure 2.3:	Four Designs of OWC (Vyzikas et al., 2017)	8
Figure 2.4:	Vertical OWC (left) and Incline OWC (right) (Iino et al., 2016)	9
Figure 2.5:	Efficiency of OWC with different inclination angles (Iino et al., 2016)	10
Figure 2.6:	Schematic Diagram of OWC with Tapered Wave Collector (Mora, Bautista and Méndez, 2017)	11
Figure 2.7:	Different OWC Chamber Front Wall Orientations (Bouali and Larbi, 2013)	12
Figure 2.8:	Average OWC efficiency against the Front Wall Immersion Depth (Bouali and Larbi, 2013)	12
Figure 2.9:	OWC with Different Chamber Bottom Profiles (Ashlin, Sundar and Sannasiraj, 2016)	13
Figure 2.10:	OWC Efficiency Variation against Ratio of Non-Immersed Chamber Length to Water Depth (Zaoui et al., 2014)	14
Figure 2.11:	Air Column Control Volume in the Chamber (Sheng, Alcorn and Lewis, 2013)	15
Figure 3.1:	Flow Chart of the Project	20
Figure 3.2:	Part 1 Project Work Plan	21
Figure 3.3:	Part 2 Project Work Plan	22
Figure 3.4:	Labels of the U-OWC Structure	23

Figure 3.5:	Dimensions of U-OWC Chamber (non-water-immersed)	24
Figure 3.6:	Dimensions of Flat Bottom Profile	24
Figure 3.7:	Dimensions of Circular Bottom Profile	24
Figure 3.8:	Dimensions of 1:1 Slope Bottom Profile	25
Figure 3.9:	Dimensions of 1:5 Slope Bottom Profile	25
Figure 3.10:	2D View and 3D View of the Water Tank	26
Figure 3.11:	3D Sketches of the Water-immersed Chamber Wall	27
Figure 3.12:	Settings of "Enclosure" Function	27
Figure 3.13:	3D View of the Water Tank Walls	27
Figure 3.14:	3D Sketches of the Non-water-immersed Chamber Wall	28
Figure 3.15:	Detail View of the Connection Points between the Non-water-immersed Part and the Water-immersed Part	28
Figure 3.16:	3D Sketches of the Chamber Orifice	29
Figure 3.17:	3D View of the Air Volume	29
Figure 3.18:	Components of the 3D Model	29
Figure 3.19:	"Water" Part	30
Figure 3.20:	"TankWall" Part	30
Figure 3.21:	"UpperChamber" Part	30
Figure 3.22:	"Air" Part	30
Figure 3.23:	Meshed 3D Model	31
Figure 3.24:	Mesh Settings	31
Figure 3.25:	Settings of Analysis Type	32
Figure 3.26:	Self-defined Expressions	33
Figure 3.27:	Water Domain (Left) and Air Domain (Right)	34

Figure 3.28: Domain Basic Settings (Left) and Domain Fluid Models (Right)	34
Figure 3.29: Initialization Settings of Air Domain	35
Figure 3.30: Initialization Settings of Water Domain	35
Figure 3.31: Location of Wall Boundary Condition of Water Domain	36
Figure 3.32: Settings for Wall Boundary Condition for Water Domain	36
Figure 3.33: Location of Inlet Boundary Condition of Water Domain	37
Figure 3.34: Settings of Inlet Boundary Condition of Water Domain	37
Figure 3.35: Location of Opening Boundary Condition of Water Domain	37
Figure 3.36: Detail View of the Opening Boundary Condition of Water Domain	38
Figure 3.37: Settings of Opening Boundary Condition of Water Domain	38
Figure 3.38: Location of Opening Boundary Condition of Air Domain	39
Figure 3.39: Settings of Opening Boundary Condition of Air Domain	39
Figure 3.40: Define of Run Settings	40
Figure 3.41: Run of Simulation	40
Figure 3.42: Choices of Plot	41
Figure 3.43: Settings of Isosurface Plot (Left) and Isosurface Plot (Right)	41
Figure 3.44: Settings of Air Vector Plot (Left) and Air Vector Plot (Right)	42
Figure 3.45: Settings of Water Vector Plot (Left) and Water Vector Plot (Right)	42
Figure 3.46: Animation Function for the Simulated 3D Model	43

Figure 3.47:	Plotted Results of Flat Bottom Profile U-OWC (Left) and Circular Bottom Profile U-OWC (Right)	43
Figure 3.48:	Plotted Results of 1:1 Slope Bottom Profile U-OWC (Left) and 1:5 Slope Bottom Profile U-OWC (Right)	43
Figure 3.49:	Function Calculators of Air Velocity (Left) and Air Pressure (Right)	44
Figure 3.50:	Equations of Average Air Velocity (Left) and Average Air Pressure (Right)	44
Figure 3.51:	Self-defined Expressions	44
Figure 3.52:	Chart Function Settings Part 1	45
Figure 3.53:	Chart Function Settings Part 2 (Left) and Chart Function Settings Part 3 (Right)	45
Figure 3.54:	Sample Air Velocity Graph	45
Figure 3.55:	Isometric View of 3D Sketch of Circular Bottom Profile U-OWC	46
Figure 3.56:	Overall View of the Prototype	47
Figure 3.57:	Water Tank	47
Figure 3.58:	Silicone Glue	47
Figure 3.59:	Faber-Castell Plasticine (Left) and Adhesive Layer of the Circular Bottom Profile (Right)	48
Figure 3.60:	U-OWC Chamber with Circular Bottom Profile	48
Figure 3.61:	Steel Enhancement Frames	49
Figure 3.62:	Overview of Arduino Water Wave Generator	49
Figure 3.63:	Circuit Diagram of Servo Motors	50
Figure 3.64:	View of Circuit Connection of Servo Motors	51
Figure 3.65:	Detail Views of Servo Motor Arm-linkages	51
Figure 3.66:	Paddles of Arduino Water Wave Generators	52
Figure 3.67:	View of Circuit Connection of Pressure Sensor	52

Figure 3.68:	Circuit Diagram of Pressure Sensor	52
Figure 3.69:	Experiment Setup	53
Figure 3.70:	Digital Vane Anemometer (Left) and Arduino Pressure Sensor (Right)	53
Figure 4.1:	Air Velocity Graph of the Flat Bottom Profile U-OWC Chamber	56
Figure 4.2:	Air Pressure Graph of the Flat Bottom Profile U-OWC Chamber	56
Figure 4.3:	Air Velocity Graph of the 1:1 Slope Bottom Profile U-OWC Chamber	57
Figure 4.4:	Air Pressure Graph of the 1:1 Slope Bottom Profile U-OWC Chamber	57
Figure 4.5:	Air Velocity Graph of the 1:5 Slope Bottom Profile U-OWC Chamber	58
Figure 4.6:	Air Pressure Graph of the 1:5 Slope Bottom Profile U-OWC Chamber	58
Figure 4.7:	Air Velocity Graph of the Circular Bottom Profile U-OWC Chamber	59
Figure 4.8:	Air Pressure Graph of the Circular Bottom Profile U-OWC Chamber	59
Figure 4.9:	Results Comparison Chart for the Simulated U-OWC Models	61
Figure 4.10:	Air Velocity Graph of the U-OWC Prototype Chamber	62
Figure 4.11:	Air Pressure Graph of the U-OWC Prototype Chamber	63
Figure 4.12:	Results Comparison Chart of Simulation and Experimental	64
Figure 4.13:	Power Output Comparison Chart of Simulation and Experimental	65
Figure 4.14:	Bending of the Paddles	66
Figure 4.15:	Positioning of the Digital Anemometer during Experiment	67

Figure 5.1:	Enhancement Frames for Tank Walls	70
Figure 5.2:	Servo Motor Arm-linkage	71

LIST OF SYMBOLS / ABBREVIATIONS

m	chamber air mass, kg
p	pressure variation, Pa
p_0	atmospheric pressure, Pa
p_c	chamber pressure, Pa
P_{PTO}	available PTO power, W
P_w	available water wave power, W
Q_w	water surface volume flow rate, m ³ /s
Q_p	air volume flow rate, m ³ /s
t	time, s
T	temperature variation, K
T_0	atmospheric temperature, K
T_c	chamber temperature, K
V	chamber air volume, m ³
V_w	water volume, m ³
$W_{pneumatic}$	pneumatic power, W
W_{wave}	water wave power, W
$\frac{d}{dt}$	differentiation with respect to time
ρ_c	chamber air density, kg/m ³
ρ_0	atmospheric air density, kg/m ³
γ	air specific heat ratio
\dot{V}	air volume flow rate, m ³ /s
CFD	Computational Fluid Dynamics
OWC	Oscillating Water Column
PTO	Power Take Off
USB	Universal Serial Bus
U-OWC	U-shape Oscillating Water Column
FYP	Final Year Project

LIST OF APPENDICES

APPENDIX A: Excel Calculation of Average Velocity of Simulation Results	76
APPENDIX B: Excel Calculation of Average Pressure of Simulation Results	78
APPENDIX C: Excel Calculation of Average Velocity of Experimental Results	80
APPENDIX D: Screenshots of Pressure Data of Experimental Results	81
APPENDIX E: Excel Calculation of Average Pressure of Experimental Results	82
APPENDIX F: Calculations of Orifice Area, Power Output and Percentage Error	83
APPENDIX G: Coding of the Servo Motor	84
APPENDIX H: Coding of the Pressure Sensor	85

CHAPTER 1

INTRODUCTION

1.1 General Introduction

World population has increased annually at an alarming rate. In 2015, a survey performed by the United Nations (UN) showed that annual growth rate of the world population is approximately 1.18 per cent or in other word, an addition of 83 million world population per year. The world population will reach 8.501 billion in 2030 and achieve 9.725 billion by 2050 (United Nations, 2015). Rapid growth of the world population causes the increase of natural resources consumption for both the renewable and non-renewable resources.

Similar to most countries, Malaysia depends principally on the fossil fuels such as the petroleum, natural gas, coal or crude oils in order to extract the required amount of energy for the industrial products, automotive applications as well as the household appliances. According to Muda and Tey (2012), the bulky mining of the fossil fuels in Malaysia has amplified the rapid reduction of fossil fuels and petroleum is expected to be mined off in 2020, natural gas will be exhausted in 2058 while coal is expected to be used up in 2066.

1.1.1 Wave Energy Potential in Malaysia

With the intentions to reduce the nation's energy usage and to decrease the oil dependency, Malaysia's government has implemented quite a number of energy policies as well as financial support for research and development on renewable energy (RE) particularly in local universities. Ocean wave energy is known as one of the potential renewable sources in Malaysia because Malaysia comprises of 2068 km of coastline in Peninsular Malaysia and 2607 km in East Malaysia (Central Intelligence Agency, 2018).

Compared with tidal energy which is generated by the gravitational pull of earth, wave energy is converted from the wind energy and the potential energy carried by the waves which have travelled for a long distance in the ocean accompanied with little energy loss. Waves can be found limitless along the shoreline during the day and the night. The continuous supply of the wave energy has provided Malaysia a great opportunity to convert the wave energy into electrical

energy. Other than that, it can be considered as the renewable energy source at low cost, environment friendly and able to reduce the dependency on fossil fuel for electricity generation.

The study performed by the Samrat et al. (2014) in which they have calculated the average power output from five locations in Malaysia that have high potential for the extraction of wave energy. It is concluded that the average wave power output from Sarawak, Sabah and Perak are 5.00 kW/m, 7.91 kW/m and 7.00 kW/m, respectively while the highest average wave power output of 15.90 kW/m can be found in Terengganu. The result of this study is shown in Table 1.1.

Table 1.1: Wave Data from Potential Locations in Malaysia (Samrat et al., 2014)

Locations	Minimum Average Wave Height (m)	Maximum Average Wave Height (m)	Average Power Output (kW/m)
Sarawak	0.59	1.56	5.00
Kota Kinabalu (Sabah)	0.43	1.66	6.50
Mabul Island (Sabah)	0.53	1.66	7.91
Pulau Mentagor Island (Perak)	0.70	1.15	7.00
Perhentian Island (Terengganu)	0.90	2.10	15.90

1.1.2 Oscillating Water Column

After about two decades of research and development on the ocean wave energy converter, oscillating water column (OWC) structure can be termed as a reliable and non-complex technology for extracting the ocean wave energy. An OWC can be built as a floating hollow structure that is floated at the offshore surface as shown in Figure 1.1 or constructed as a fixed structure that is installed at the onshore cliff as shown in Figure 1.2. OWC consists of two major components, namely the wave collecting chamber and the power take off (PTO) system.

For both types of the OWC, the wave collecting chamber is immersed below the sea water and this creates a volume of air trap in between the inner water surface and the PTO system. The rise and fall of the ocean wave will increase and decrease the water column level in the OWC chamber. With the compression and decompression of the air, the PTO turbine will rotate and convert the mechanical

energy into electrical energy. Thereafter, the generated electricity can be supplied to the power grid.

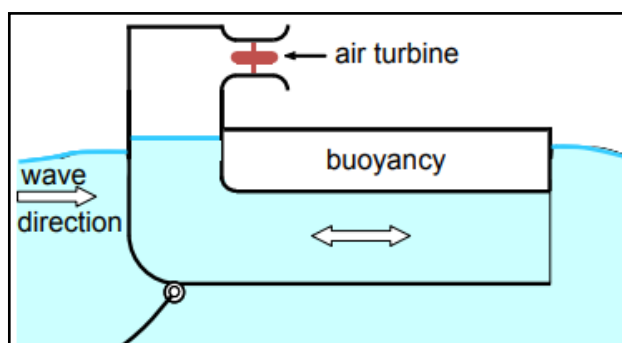


Figure 1.1: Schematic Diagram of an Offshore OWC (Falcão and Henriques, 2016)

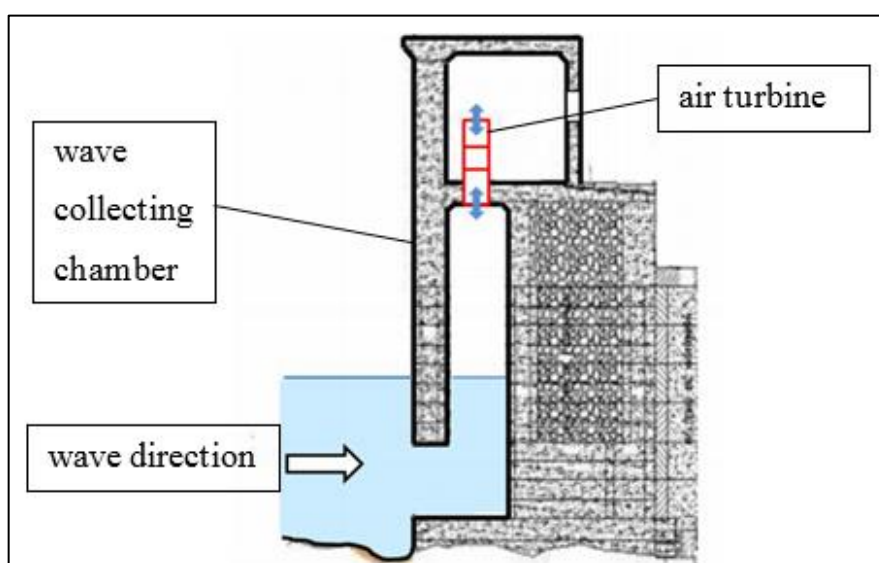


Figure 1.2: Schematic Diagram of an Onshore OWC (Falcão and Henriques, 2016)

1.2 Importance of the Study

The results of this present study may have significant impact on maximizing the power output from the U-shape Oscillating Water Column (U-OWC) with the optimization of the chamber bottom profile. Besides, the study may provide guidelines for the construction of the OWC prototype as well as contribute to a better understanding of fundamental theory behind the OWC which includes:

- i. The mechanisms of OWC on the wave collection and energy conversion.
- ii. The efficiency of the OWC with respect to the structure parameters.
- iii. Fluid analysis on the OWC prototype 3D model.

1.3 Problem Statement

In recent years, researches about the optimum OWC shape have been performed to maximize the OWC power output. One of the prominent findings is the U-OWC, which is found to have greater power efficiency as compared to conventional OWC (Vyzikas et al., 2017). According to the finding by Mora, Bautista and Méndez (2017), the air-discharge velocity of the OWC could be maximized with the implementation of tapered and slender wave collector.

Although the overall structure of OWC has been popularly used as research topic in the field of the wave energy, its internal detailed structure has rarely been explored. Currently, there are few studies on the internal structure of the OWC and the only study was conducted by Ashlin, Sundar and Sannasiraj (2016) on the shape optimization of the OWC bottom profile for the conventional OWC structure. Therefore, it is of interest to perform simulation test and experimental validation to determine the power efficiency improvement from the optimum bottom profile for U-OWC structure.

1.4 Aim and Objectives

The main aim of this study is to determine the optimum bottom profile for the U-OWC structure that can provide the best performance of U-OWC. The specific objectives of this research are:

- i. To investigate the effects of different bottom profiles on the U-OWC power output in terms of air-discharge velocity via 3D model simulation of the U-OWC by using ANSYS CFX software.
- ii. To fabricate the U-OWC prototype based on the optimised bottom profile as simulated.
- iii. To evaluate the power efficiencies via simulation and experimental for the establishment of the optimum bottom profile of U-OWC.

1.5 Scope and Limitation of the Study

The working scope of this study is to determine the best configuration of the U-OWC bottom profile by using the ANSYS CFX simulation software and the evaluation of the actual experimental result is based on a U-OWC prototype. In the simulation process, the U-OWC bottom profile will be varied with four different configurations which are derived based on the study from Ashlin, Sundar and Sannasiraj (2016)

namely, the flat bottom, the circular bottom, the 1:1 slope and the 1:5 slope. Some limitations are recognised such as:

- i. The experimental water wave will not behave as the actual ocean wave fluctuation pattern and this may cause the occurrence of non-optimum power output measurement.
- ii. The geometry similarities of the OWC prototype and the 3D model OWC would be slightly varied due to the limitation of workmanship and fabrication tool (Falcão and Henriques, 2014).
- iii. The experimental result of predicted power output of U-shape OWC prototype may be affected by the scale effects namely the air compressibility and non-linearity (Simonetti et al., 2017).

1.6 Contribution of the Study

The optimum design of U-OWC bottom profile as concluded in this study may help to improve the power efficiency of the future OWC structures. Moreover, theories and techniques which are involved during the study may contribute in supporting information to the future research projects on the parametric optimization of U-OWC.

1.7 Outline of the Report

This report is succeeded by Chapter 2 where literature reviews are presented and commented. Chapter 3 describes the methodology and work plan of this study. After that, Chapter 4 presents the simulation and experimental results along with some discussions. Lastly, conclusion and recommendations of this study are presented in Chapter

CHAPTER 2

LITERATURE REVIEW

2.1 Introduction

The main focus of this study is the onshore permanent oscillating water column (OWC). In order to gain a better understanding towards the parametric optimization of the OWC, the related research findings will be discussed. First and foremost, the structure and principal operation of the OWC will be explained. Subsequently, the optimum overall shape of the OWC, parametric optimization of the OWC chamber will be reviewed. After that, the air and wave theories will be acknowledged. Subsequently, the operation of the ANSYS Computational Fluid Dynamics and the relationship between the numerical and experimental methods will be reviewed in the last section.

2.2 Operation of OWC

OWC is built by two important components which are the (i) wave collecting chamber and (ii) power take-off system (PTO). The wave collecting chamber is hollow and it is semi-submerged below the sea level. With the alternating wave motions of rise and fall, the mechanism of the trapped air above the water column inside the wave collecting chamber can be modelled as the piston (Shalby, Walker and Dorrell, 2017). The rise of the water column will expel the trapped air through the top opening of the chamber while the fall of the water column will draw air into the chamber.

In the meantime, the continuous movement of high air velocity will drive the PTO system and thus the pneumatic energy is converted into electrical energy. The electricity generation of the PTO system is able to occur continuously because the PTO system is equipped with the bidirectional turbine which rotates only in a single direction regardless of the air flow direction through the turbine (Torre-Enciso et al., 2009). The operations explanation are illustrated in Figure 2.1.

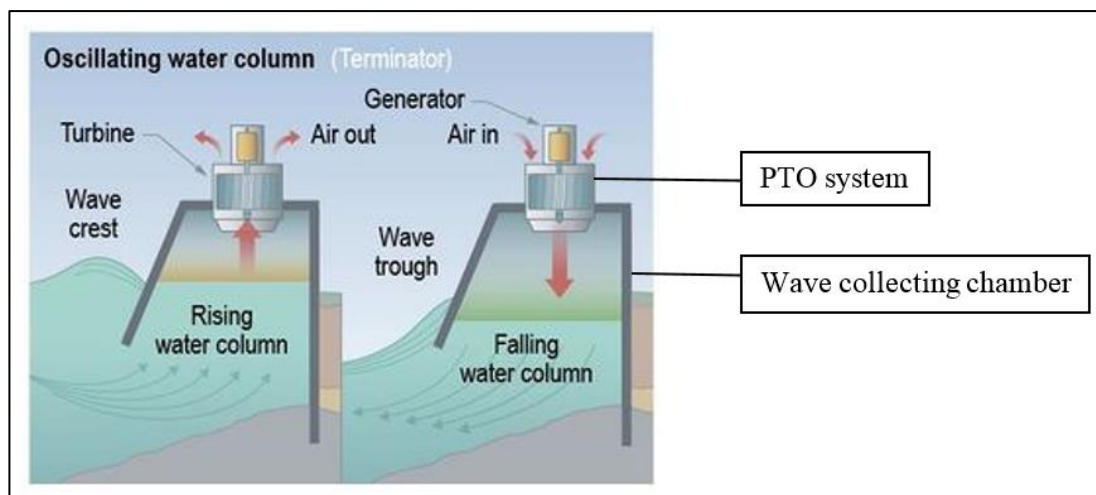


Figure 2.1: Mechanisms of an Onshore Fixed OWC (Office of Energy Efficiency & Renewable Energy, 2018)

2.3 Performances of OWC with Different Shapes

Various studies (Boccotti, 2007; Vyzikas et al., 2017; Falcão and Henriques, 2016; Simonetti et al., 2017; Mora, Bautista and Méndez, 2017) indicate that the overall shape of the OWC can significantly affect the power efficiency of the OWC. In these years, the popular configurations of the OWC that have been studied and investigated included the vertical, the slanted and the U-shape.

2.3.1 Comparison of U-OWC and Conventional OWCs

The performances of the conventional OWC and the U-OWC as sketched in Figure 2.2 were compared in the study of Boccotti (2007). Notably, the finding confirms the extended breakwater structure of the U-OWC can cause the water wave to induce higher vertical force through the chamber opening. This results the vertical acceleration of U-OWC water column to be 13 % greater than that of the conventional OWC. Conversely, the wave amplification factor of the U-OWC is 2.5 % lower than that of the conventional OWC.

Boccotti (2007) concluded that although the U-OWC has a lower wave amplification, its good performance is assured by its greater values in the wave column acceleration, the resonant period and the amplitude of pressure fluctuations. These qualities of the U-OWC happen because U-OWC has a higher opening which is nearer to the water surface than the conventional OWC.

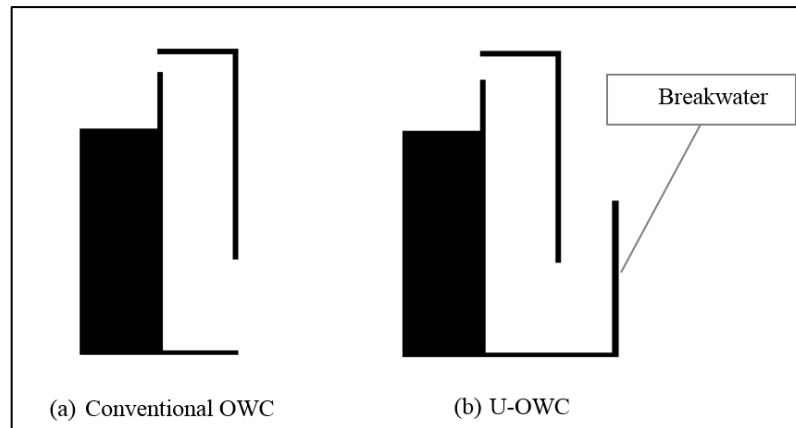


Figure 2.2: Schematic Diagram of OWCs

The finding by Boccotti (2007) was a major breakthrough in the development of the OWC which supports the statement on U-OWC can provide greater power output than that of the conventional OWC.

Eventually, the U-OWC was modified by Vyzikas et al. (2017). Feature of the slope was implemented on the conventional OWC and U-OWC to create the four models as shown in Figure 2.3. In fact, Model 1 in Figure 2.3 is the U-OWC proposed by the Boccotti (2007) and the Model 3 in Figure 2.3 is the conventional OWC. The addition of slope for Model 2 in Figure 2.3 is to behave like an actual sea bottom where the impurities are saturated in front of the U-OWC. While the Model 4 in Figure 2.3 applies the same idea as Model 2 but with the conventional OWC.

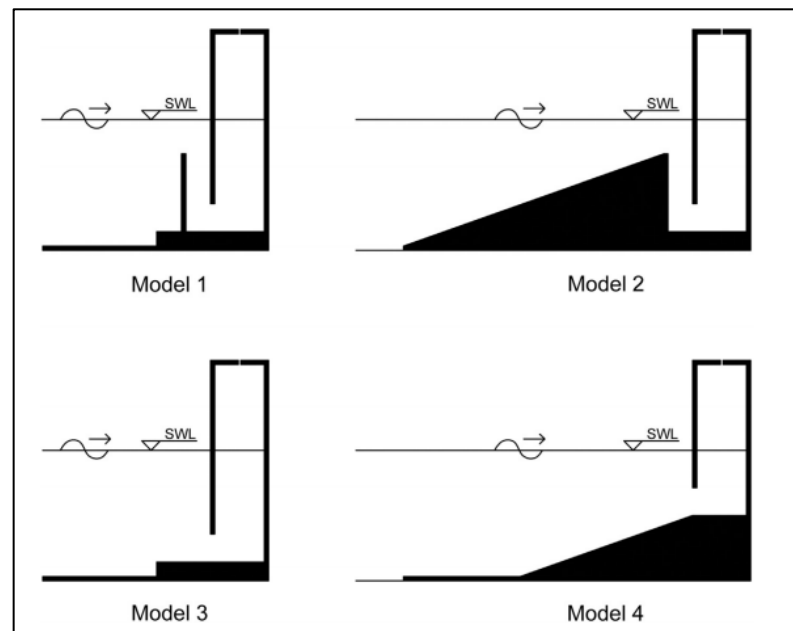


Figure 2.3: Four Designs of OWC (Vyzikas et al., 2017)

Vyzikas et al. (2017) tested all the models with regular and irregular wave with respect to range of frequency from 0.3 Hz to 0.7 Hz and the capture efficiency for each model was recorded. The experimental results indicated that the capture efficiency of the Model 1 and Model 2 are greater than that of the Model 3 and Model 4 in both of the regular wave and irregular wave conditions. The increasing order of the OWC performance is found to be Model 3, Model 4, Model 1 and Model 2. Given these points, the efficiency of the conventional OWC and the U-OWC can be enhanced by the implementation of the slope feature respectively and the ‘toe-protected’ U-OWC has the best performance among all the models.

2.3.2 Effects of Incline Orientation on OWC

Inclination effect of OWC chamber was tested by Iino et al. (2016). The schematic diagram of the vertical OWC and incline OWC is illustrated in Figure 2.4. The experiment investigated the efficiency of OWC with respect to chamber inclination angle of 18.4° , 45° and 90° .

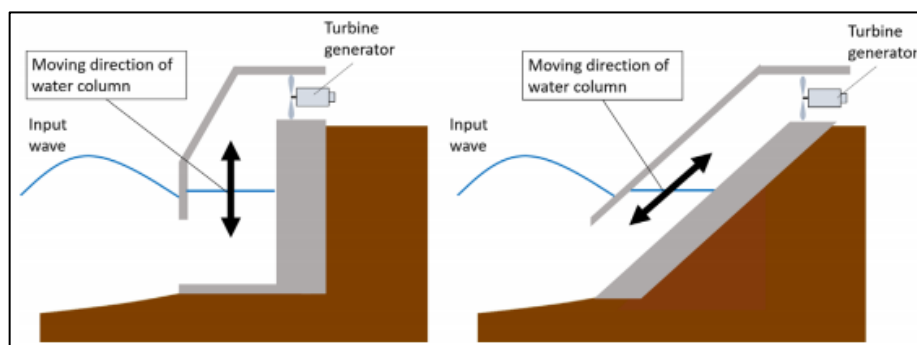


Figure 2.4: Vertical OWC (left) and Incline OWC (right) (Iino et al., 2016)

Iino et al. (2016) discussed that the rise of inclination angle causes the mass of the water column to increase. The phenomena is due to the incline chamber that changes the motion direction of the OWC and hence reduces the gravity effect on the water column. As a result, the natural oscillation period of the OWC is enlarged. Moreover, Iino et al. (2016) found that 45° inclination angle can provide the highest OWC efficiency among all the inclination angles as shown in Figure 2.5.

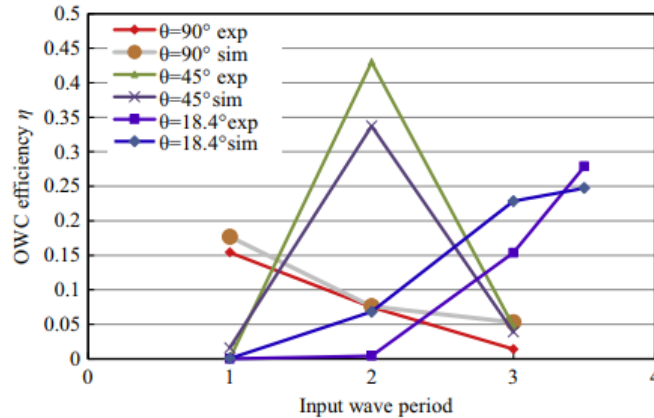


Figure 2.5: Efficiency of OWC with different inclination angles (Iino et al., 2016)

As a supporting point for the finding by (2016), LIMPET report (The Queen's University of Belfast, 2002) has proved that the actual operating OWC with an inclination angle of 40° has higher power efficiency than the vertical OWC because the incline chamber creates more plane area for water column. Consequently, the occurrence of turbulence is reduced, power loss is minimized and hence the resonant period is extended.

2.3.3 Wave Collector

The effect of tapered wave collector on OWC was studied by Mora, Bautista and Méndez (2017). Two parameters were important in affecting the OWC capture efficiency namely, the OWC structure width, $2H$ and the wave collector width, b_2 . The experimental OWC schematic diagram is illustrated in Figure 2.6.

Mora, Bautista and Méndez (2017) claimed that the decrement in ratio of $2H$ to b_2 will enlarge the water waves potential energy and the wave amplitude inside the OWC chamber. Henceforth the air-velocity discharge is improved and specifically, when the b_2 is 4 times greater than the $2H$, the air-velocity discharge is amplified with a factor of 2. As a result, the capture efficiency of OWC can be improved by implementing the tapered wave collector.

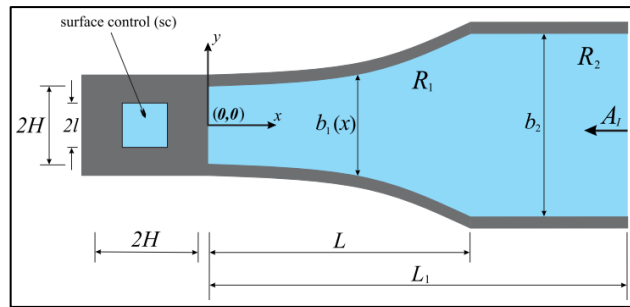


Figure 2.6: Schematic Diagram of OWC with Tapered Wave Collector (Mora, Bautista and Méndez, 2017)

2.4 Parametric Optimization of OWC

Apart from the studies regarding the optimal overall shape of the OWC, effects of internal and external parameters of the OWC have been studied by several studies, (Bouali and Larbi, 2013; Mora, Bautista and Méndez, 2017; Ashlin, Sundar and Sannasiraj, 2016; Zaoui et al., 2014). The focus of studies include the chamber front wall orientation, chamber front wall immersion depth, chamber bottom profile as well as the orifice location.

2.4.1 Chamber Front Wall Orientation

Bouali and Larbi (2013) performed ANSYS-CFX simulation to investigate the effect of OWC front wall orientations on the OWC efficiency. Five orientations were tested as demonstrated in Figure 2.7. The front walls possess angle of deviation from the water surface which are 90° , 45° , -45° , 0° and 180° respectively.

Case 4 front wall orientation with the front wall tip of the flow direction is found to be the optimum orientation with maximum average efficiency of 16.97%. This 0° deviated front wall provides the highest air pressure on the water column and causes the ultimate OWC free surface oscillation. While the second best orientation is the Case 5 which has 1.12 times lower average efficiency than that of the Case 4 front wall orientation.

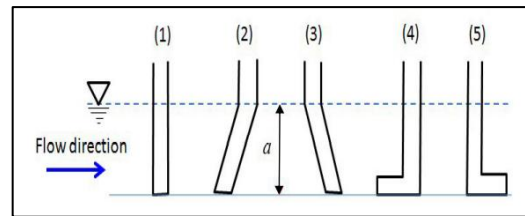


Figure 2.7: Different OWC Chamber Front Wall Orientations (Bouali and Larbi, 2013)

2.4.2 Chamber Front Wall Immersion Depth

Based on the experiment done by Mora, Bautista and Méndez (2017), ratio of front wall immersion depth to the water depth was varied in order to determine the optimum OWC efficiency. In specific, the ratios are 0.2, 0.3, 0.4 and 0.5. The results indicate that the increase in immersion depth will cause the increments in water column air pressure and the air-velocity discharge. Accordingly, the front wall immersion depth which is 50 % of the water depth yields the maximum OWC efficiency.

However, Bouali and Larbi (2013) claimed that the peak OWC efficiency of 24.53 % can only be obtained by setting the front wall immersion depth to be 40 % of the water depth. The effect of the front wall immersion depth on the OWC is tabulated in Figure 2.8. For the given points, it can be concluded that the optimum range for the ratio of front wall immersion depth to water depth is 0.4 to 0.5.

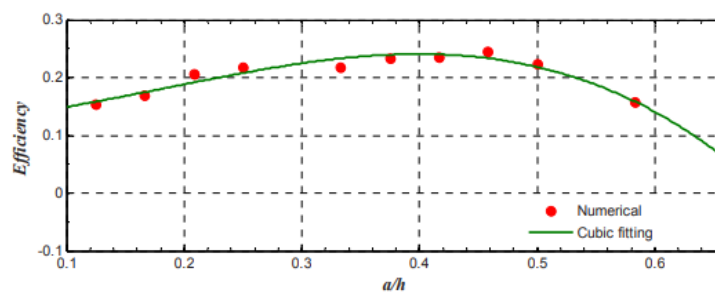


Figure 2.8: Average OWC efficiency against the Front Wall Immersion Depth (Bouali and Larbi, 2013)

2.4.3 Chamber Inner Bottom Profile

Ashlin, Sundar and Sannasiraj (2016) conducted an experiment to investigate the OWC chamber bottom profile with four different configuration which are slope of 1:5, slope of 1:1, circular curve and flat as shown in Figure 2.9. It is found that all the

four different configurations provide the similar OWC efficiency in the random water wave condition. Whereas the OWC with circular bottom profile has outperformed the other three configurations which generates the maximum efficiency in the regular water wave condition.

In terms of hydrodynamic efficiency, the descending order of the bottom profiles is the circular bottom, slope of 1:5, flat and slope of 1:1. Ashlin, Sundar and Sannasiraj (2016) explained that the circular bottom profile yields the highest OWC efficiency because the circular curve smoothen the entry of water wave motion and thus, increases the water surface oscillation in the chamber. The enhancement of the water wave amplification factor results greater air volume compression and eventually, the high air-velocity discharge is generated.

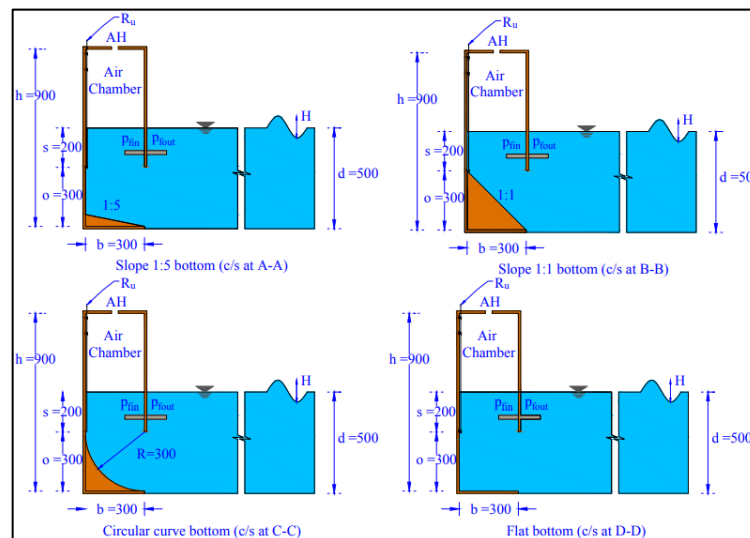


Figure 2.9: OWC with Different Chamber Bottom Profiles (Ashlin, Sundar and Sannasiraj, 2016)

2.4.4 Chamber Length

According to Zaoui et al. (2014), the geometry of OWC chamber length was studied through the ANSYS CFD. The simulation result shows that the maximum OWC efficiency is achieved when the non-immersed chamber length is a quarter of the water depth. Whereas the OWC efficiency will be reduced significantly if the ratio of the non-immersed chamber length to water depth is lesser than 0.225. The efficiency trend against the variation of non-immersed chamber length is plotted in Figure 2.10.

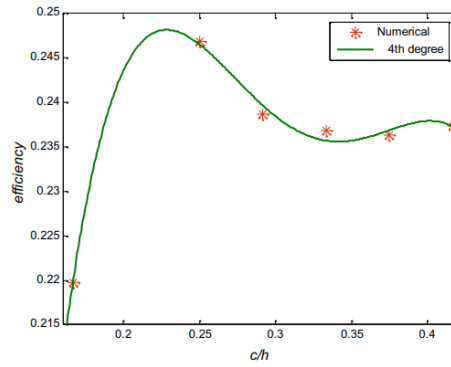


Figure 2.10: OWC Efficiency Variation against Ratio of Non-Immersed Chamber Length to Water Depth (Zaoui et al., 2014)

2.4.5 Orifice Dimension

The optimum OWC efficiency of 0.24 can be achieved when the ratio of the section area of orifice to water column surface is 0.0081 (Zaoui et al., 2014). However, Hsieh et al. (2012) claimed that the optimum ratio is 0.0121. It is explained that the orifice section area should not be too small for the small-scale OWC because it would result the effect of air compressibility in the OWC chamber which is contradict to the ideal incompressible air condition.

2.5 Power Conversion of OWC

Based on the study performed by Sheng, Alcorn and Lewis (2013), the thermodynamic process in the OWC chamber composes of two main processes which are inhalation and exhalation. With the assumption of uniform air in the OWC chamber, the air state parameters namely, the pressure, density and temperature in both the inhalation and the exhalation processes are equal. The air uniformity results the conditions as shown in Equation (2.1) and Equation (2.2).

$$p_c = p + p_0 \quad (2.1)$$

$$T_c = T + T_0 \quad (2.2)$$

The parameters, p_c and T_c are the chamber pressure and chamber temperature respectively. p and T are termed as the chamber pressure variation and chamber temperature variation while the p_0 and T_0 are the atmospheric pressure and ambient temperature.

During the inhalation process, the chamber air undergoes decompression which causes the chamber pressure to be lesser than the atmospheric pressure, hence the ambient air flows into the chamber with the condition, $p < 0$. Whereas during the exhalation process, the chamber air undergoes compression which causes the chamber pressure to be greater than the atmospheric pressure, hence the chamber air flows out from the chamber with the condition, $p > 0$.

In order to study the thermodynamic system of the OWC, the air column inside the chamber can be converted into a 2D control volume which consist of 4 boundaries as shown as in Figure 2.11.

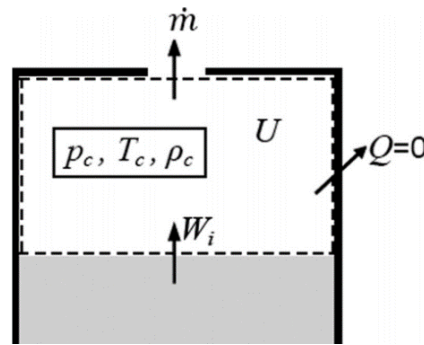


Figure 2.11: Air Column Control Volume in the Chamber (Sheng, Alcorn and Lewis, 2013)

Without the assumption of adiabatic process, the inhalation and the exhalation processes are expected to face heat energy loss through the left boundary and the right boundary. Work done by the water wave to the air column is happened through the bottom boundary which can mathematical expressed as the multiplication of pressure chamber and the volume change rate of water wave in the chamber:

$$W_{wave} = p_c \times \frac{dV_w}{dt} \quad (2.3)$$

where

W_{wave} = water wave power, W

$\frac{dV_w}{dt}$ = water volume change rate, m³/s

The work done by the air column to the PTO component through the top boundary causes the generation of air mass flow. Subsequently, the pneumatic power can be calculated with the product of chamber pressure and the air volume flow rate which is expressed as:

$$W_{pneumatic} = p_c \times \dot{V} \quad (2.4)$$

where

$W_{pneumatic}$ = pneumatic power, W

\dot{V} = air volume flow rate, m³/s

With the application of Thermodynamic First Law and adiabatic process assumption, the expression of air mass rate is derived as

$$\frac{dm}{dt} = \rho_c \frac{dV}{dt} + V \frac{d\rho_c}{dt} \quad (2.5)$$

where

m = chamber air mass (time dependent)

ρ_c = chamber air density, kg/m³

V = chamber air volume, m³

In this context, inhalation will result the positive air mass rate while the exhalation will result the negative air mass rate.

Taking the consideration of compressibility effect, air density will vary in the inhalation and the exhalation. In precise, inhalation draws the atmospheric air into the chamber whereas exhalation expels the pressurized air from the chamber. Hence, the air volume flow rate is expressed in a different way:

$$Q_{p(inhalation)} = -\frac{1}{\rho_0} \frac{dm}{dt} \quad (2.6)$$

$$Q_{p(exhalation)} = -\frac{1}{\rho_c} \frac{dm}{dt} \quad (2.7)$$

where

Q_p = air volume flow rate, m³/s

ρ_0 = atmospheric air density, kg/m³

The water surface volume flow rate can be expressed as:

$$Q_w = - \frac{dV}{dt} \quad (2.8)$$

where

Q_w = water surface volume flow rate, m³/s

Consequently, the available PTO output power and available water wave input power can be calculated by the mathematical equations:

$$P_{PTO} = pQ_p \quad (2.9)$$

$$P_w = pQ_w \quad (2.10)$$

where

P_{PTO} = available PTO power, W

P_w = available water wave power, W

2.5.1 Incompressible Air

In the small scale OWC, incompressible air state occurs due to the effects of small pressure and small air volume. When the air is incompressible, the air density will be equal in the inhalation and exhalation. Thus, the air mass change through the PTO will be solely controlled by the air volume change rate as demonstrated in Equation 2.11 and leads to the equal magnitude for the PTO power and water wave power as in Equation 2.12.

$$Q_p = - \frac{1}{\rho_c} \frac{dm}{dt} = - \frac{dV}{dt} = Q_w \quad (2.11)$$

$$P_w = P_{PTO} \quad (2.12)$$

2.5.2 Ideal Air

The assumption of isentropic can be made to simplify the power conversion in the chamber. The density and temperature equations are resulted as shown in Equation 2.13 and Equation 2.14 respectively.

$$\rho_c = \rho_0 \left(1 + \frac{p}{\gamma p_0}\right) \quad (2.13)$$

$$T_c = T_0 \left(\frac{\gamma-1}{\gamma}\right) \left(\frac{p}{p_0}\right) \quad (2.14)$$

where

γ = air specific heat ratio

As a result, the equations of air volume flow rate for inhalation and exhalation are simplified as shown in Equation 2.15 and Equations 2.16 accordingly.

$$Q_{p(inhalation)} = \left(1 + \frac{p}{\gamma p_0}\right) Q_w - \frac{V}{\gamma p_0} \frac{dp}{dt} \quad (2.15)$$

$$Q_{p(exhalation)} = Q_w - \frac{V}{\gamma p_0 + p} \frac{dp}{dt} \quad (2.16)$$

2.6 ANSYS Computational Fluid Dynamics

ANSYS Computational Fluid Dynamics (CFD) is a software that is used to simulate the OWC prototype models in the present study. Where CFD is a numerical method on the investigation of the structure-fluid interaction based on the variation of the flow characteristics, such as pressure, temperature, density and velocity. The fluid flow case problem is solved through mass continuity equation, Navier-Stokes equation and energy equation. Subsequently, the engineering effects due to the fluid flow are determined, for instance, stress, strain and pressure drop (Sharma, 2017).

The necessary steps for the ANSYS CFD simulation process are,

1. Geometry: 3D modeling of the structure which undergoes interaction with fluid flow. The sketching can be done by the CAD software such as ANSYS Design Modeler or Solidworks.
2. Mesh: The 3D model is decomposed into cells while the faces and grid points are formed to hold contact with the adjacent cells. The available 3D meshes

include tetrahedron, hexahedron, wedge, pyramid and polyhedral (SAS IP Incorporated, 2018). Appropriate meshing size can avoid divergence of the numerical solution.

3. Setup: Physical properties such as material, mass and stiffness of the 3D model are defined. Flow type is selected together with the settings of external boundary and internal boundary conditions such as pressure outlet, wall boundary and axis boundary. Furthermore, step size and number of iteration are defined as the convergence criteria for the simulation.
4. Solver: The CFD simulation is started and the computational speed is mainly affected by mesh size, step size and the capability of computer hardware. In specific, the higher the setup complexity, the longer the processing time.
5. Results: The simulation results can display the calculations of convergence parameters in terms of stream function and vorticity. Engineering parameters such as stress, shear, strain and velocity can be expressed accordingly with 3 types of visualization. In specific, 1D data can be shown by straight line function, 2D data is extracted through streamlines and contours with colour diagrams whereas the 3D data is obtained through the cutlines, cutplanes and isosurfaces (SAS IP Incorporated, 2018).

2.7 Summary

Literature review provides the information on OWC mechanisms of inhalation and exhalation. Several points regarding the overall shape of OWC are summarized. The U-OWC is proved to have greater efficiency than the conventional OWC. Efficiency of the U-OWC can be enhanced by the addition of slope at the front wall of U-OWC. The inclination angle from 40° to 45° of chamber can increase the OWC efficiency. The tapered wave collector can improve the OWC efficiency.

Apart from that, the efficiency of the OWC can be increased with several chamber modifications which are the front wall with extruded part opposes to the flow direction and circular curve bottom profile. Furthermore, the optimum front wall immersion depth, appropriate chamber length and ideal orifice dimension are discussed. Thereafter, power conversion from the water wave to the PTO is explained with the assumptions of adiabatic and incompressible air and followed by the review of ANSYS CFD simulation steps.

CHAPTER 3

METHODOLOGY AND WORK PLAN

3.1 Introduction

The work plan of the present study is presented in Figure 3.1. The project begins with the research process which performs the literature review in Chapter 2. Selection of the optimum U-OWC bottom profile and the evaluation of simulation and experimental results are presented in Chapter 4. Whereas Chapter 3 describes the three crucial phases that comprises design phase, simulation phase and experimental phase.

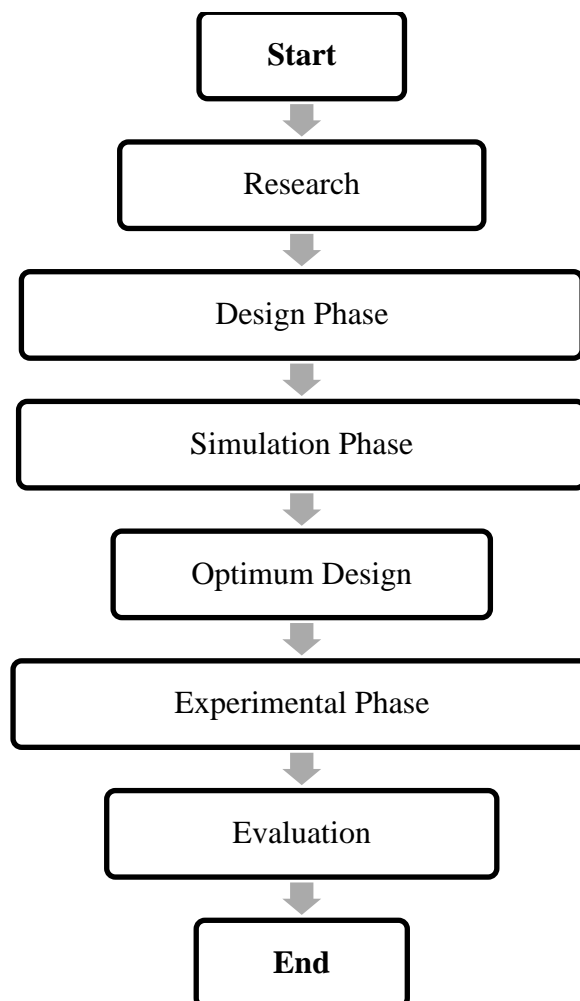


Figure 3.1: Flow Chart of the Project

3.2 Work Plan

The project is divided into two parts for two semesters respectively. Each semester consists of fourteen weeks. Part 1 project begun with project planning for one week and followed by information gathering and introduction writing for about five weeks. Articles about the OWC were studied and were discussed in literature review for about five weeks. The 3D modelling of the U-OWC with four different bottom profiles has used about four weeks. Finalization of the progress report was completed two weeks before the end of semester. Submission of progress report and Part 1 presentation was completed in the final week. Figure 3.2 displays the Gantt Chart for Part 1 project.

Project Activities	W1	W2	W3	W4	W5	W6	W7	W8	W9	W10	W11	W12	W13	W14
Project Planning														
Research & Introduction														
Literature Review														
Design Phase														
Report Writing														
Report Submission & Presentation														

Figure 3.2: Part 1 Project Work Plan

Part 2 project was started with the three weeks' process of ANSYS CFX simulation on the four U-OWC 3D models with four different bottom profiles. After the optimum design was determined based on the simulation result, the optimal bottom profile of U-OWC prototype was fabricated in two weeks period. Along with the fabrication of the optimum U-OWC prototype, the construction of Arduino water wave generator was started and was completed in five weeks period. One week was

used for the experimental phase to obtain the air-discharge velocity of the U-OWC prototype. The experimental results were compared to the simulation results and been discussed for about three weeks. Finalization of the final report has costed about two weeks' time. Submission of final report and Part 2 presentation were completed in the final week. Figure 3.3 displays the Gantt Chart for Part 2 project.

Project Activities	W1	W2	W3	W4	W5	W6	W7	W8	W9	W10	W11	W12	W13	W14
Simulation														
Optimum Design Fabrication														
Arduino Water Wave Generator Construction														
Experimental Phase														
Result & Discussion														
Report Writing														
Report Submission & Presentation														

Figure 3.3: Part 2 Project Work Plan

3.3 Design Phase

This section presents the designs and the dimensions of the four U-OWC bottom profiles specifically, flat, circular, slope of 1:1 and slope of 1:5. The purpose of this phase is to provide the U-OWC dimensions for the 3D Modelling process in the ANSYS CFX software.

3.3.1 Optimum Dimensions of U-OWC

The geometry of the optimum U-OWC structure was determined based on the research conducted by Malara et al. (2017). The optimized dimensions of U-OWC are shown in the second column of Table 3.1. The optimized dimensions were scaled

down with the multiplication factor of 0.04 in order to provide a reasonable U-OWC size that can be fabricated for experimental purpose. The scaled-down dimensions of the optimum U-OWC are shown in the third column of Table 3.1.

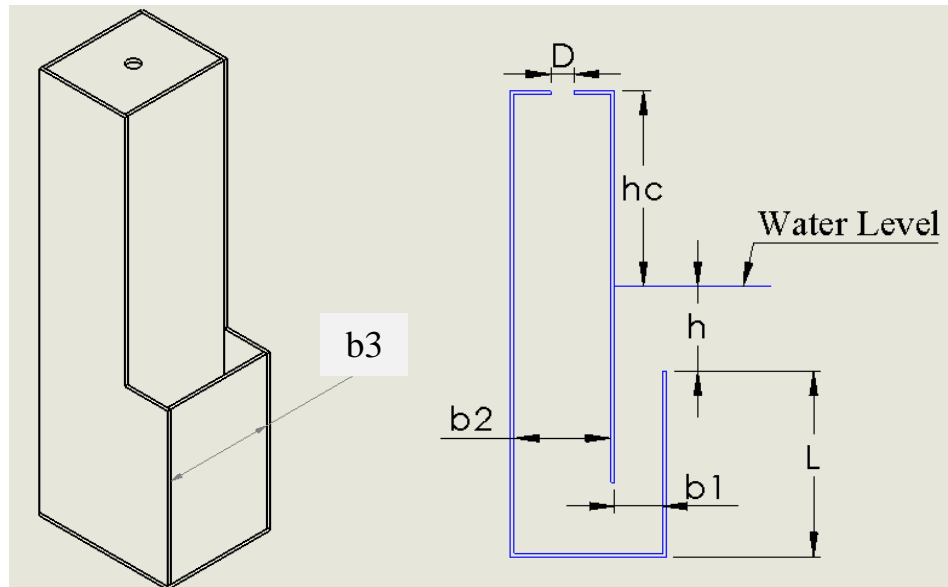


Figure 3.4: Labels of the U-OWC Structure

Table 3.1: Dimensions of Optimum U-OWC with multiplication factor of 0.04

Label	Optimum Dimension (m)	Scaled-down Dimension (cm)
b1	1.60	6.40
b2	3.20	12.80
b3	3.90	15.60
D	0.70	2.80
h	2.00	8.00
hc	9.40	37.6
L	6.25	25.00

3.3.2 Dimensions of the Different Bottom Profiles

In order to match the dimensions of the flat bottom profile U-OWC prototype which was retrieved from the former FYP project, the dimension parameters of D was slight increased to 3 cm and h was enlarged to 13.5 cm. Afterwards, these finalized dimensions of the U-OWC chamber were split into water-immersed part as shown in Figure 3.5 and non-water-immersed part for the four bottom profiles of flat (Figure 3.6), circular (Figure 3.7), 1:1 slope (Figure 3.8) and 1:5 slope (Figure 3.9) respectively. The separation of the chamber dimensions was to categorize the air

domain and the water domain and to ease the process of fluid domain declaration in ANSYS CFX Setup. Further information will be explained in Chapter 3.4.3.2.

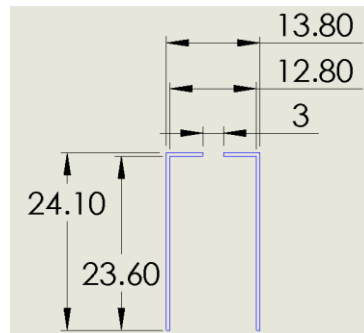


Figure 3.5: Dimensions of U-OWC Chamber (non-water-immersed)

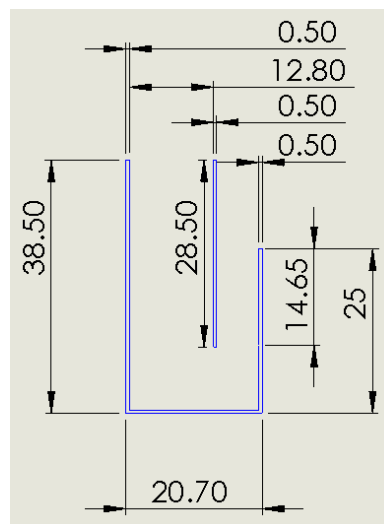


Figure 3.6: Dimensions of Flat Bottom Profile

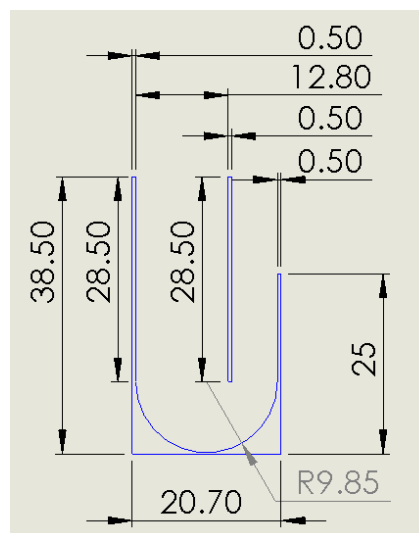


Figure 3.7: Dimensions of Circular Bottom Profile

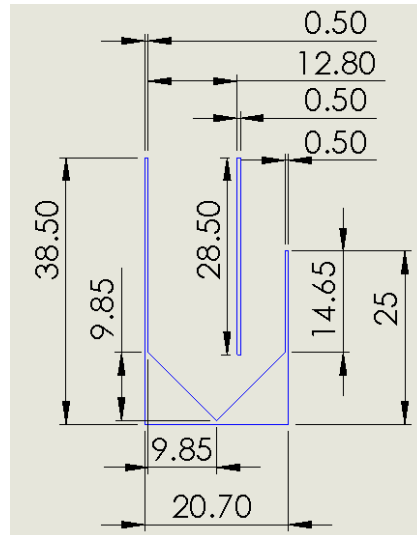


Figure 3.8: Dimensions of 1:1 Slope Bottom Profile

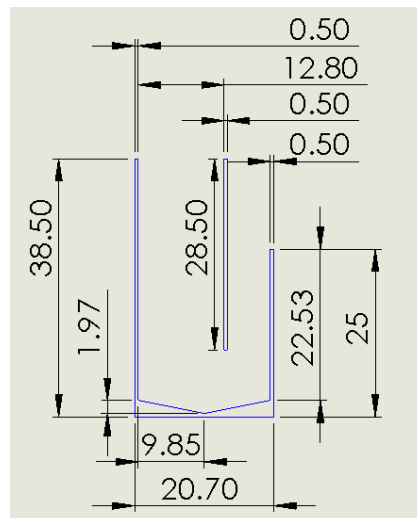


Figure 3.9: Dimensions of 1:5 Slope Bottom Profile

3.4 Simulation Phase

ANSYS CFX 17 software was implemented to conduct structure-fluid simulation on the four different U-OWC bottom profiles as presented in Chapter 3.3.2, specifically flat, circular, slope of 1:1 and slope of 1:5. The five sequential steps for the simulation phase are 3D Modeling, Meshing, Setup, Solution Generation and CFD-Post Result. Notably, the flat bottom profile U-OWC is taken as the demonstration sample for the simulation processes. Therefore, the four U-OWC models will undergo the same simulation settings as explained in this sub-chapter except the geometry sketching.

3.4.1 3D Modeling

ANSYS Design Modeler is a built-in 3D sketching software in ANSYS CFX 17 software. All U-OWC 3D models were sketched with this software.

3.4.1.1 Water Tank

The first step was to sketch the water tank of the U-OWC and the dimensions of the water tank were set to be 120 cm (length), 30 (width) and 39 cm (height) as referred to the real water tank prototype which was retrieved from the former FYP project. The conversion of 2D sketch to 3D sketch was performed by the “Extrude” function. The purpose of this 3D sketch is to create the water volume that will be used to allocate the U-OWC chamber. Figure 3.10 shows the detail views of the water tank.

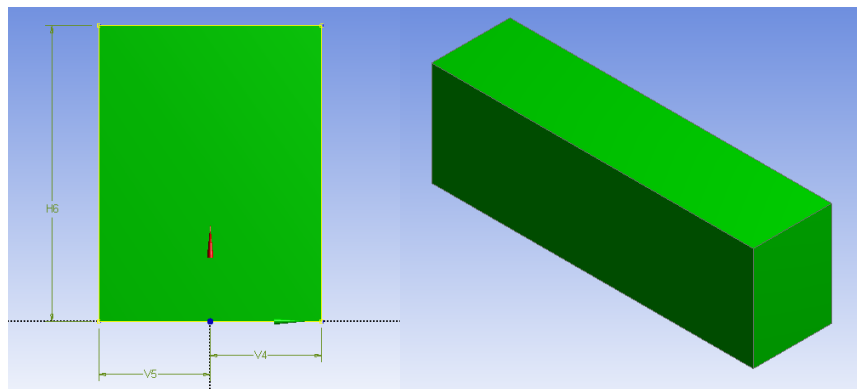


Figure 3.10: 2D View and 3D View of the Water Tank

3.4.1.2 Water-immersed U-OWC Chamber Part

After the completion of water tank, a series sets of plane creation, 2D geometry sketching and “extrude cut material” function were performed to 3D sketch the walls of water-immersed part of U-OWC chamber. The process is illustrated in Figure 3.11.

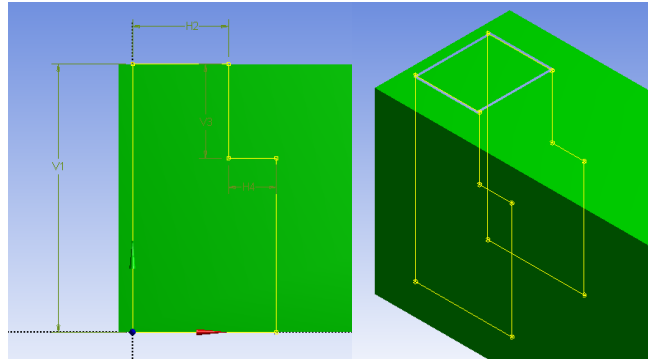


Figure 3.11: 3D Sketches of the Water-immersed Chamber Wall

3.4.1.3 Water Tank Walls

“Enclosure” function was performed to create the 0.5 cm thickness of water tank walls. Hence, the “cushion values” for the “enclosure” setting were set to 0.5 cm as shown in Figure 3.12. The 3D sketch of the water tank walls is displayed in Figure 3.13.

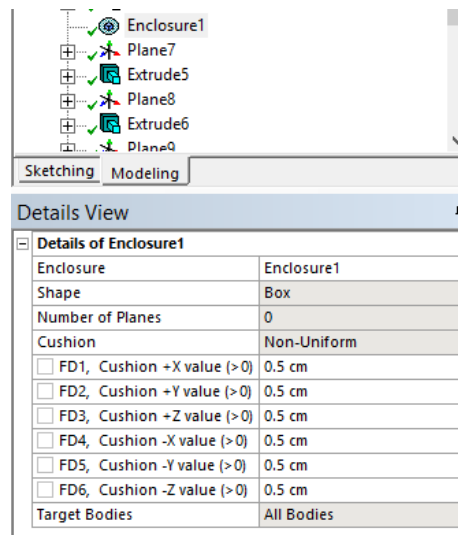


Figure 3.12: Settings of "Enclosure" Function

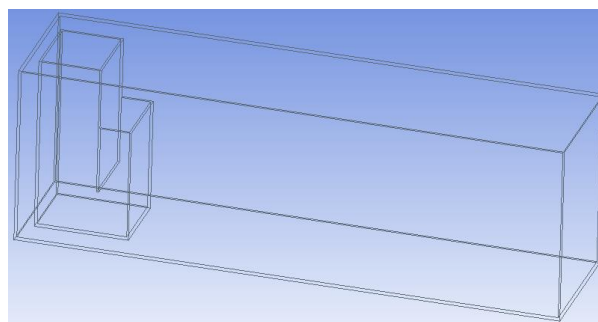


Figure 3.13: 3D View of the Water Tank Walls

3.4.1.4 Non-water-immersed U-OWC Chamber Part

After the completion of water tank, tank walls and water-immersed chamber walls, a series sets of plane creation, 2D geometry sketching and “extrude add material” function were performed to 3D sketch the walls of non-water-immersed part of U-OWC chamber. The process is illustrated in Figure 3.14. A very important point to be acknowledged during in this part is that the connection points between the non-water-immersed part and the water-immersed part must be matched perfectly to ensure the software can recognizes the chamber as a whole body. The detail view of the connection points is shown in Figure 3.15.



Figure 3.14: 3D Sketches of the Non-water-immersed Chamber Wall

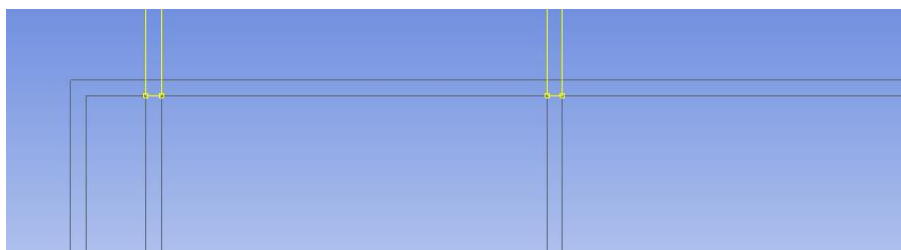


Figure 3.15: Detail View of the Connection Points between the Non-water-immersed Part and the Water-immersed Part

3.4.1.5 Chamber Orifice

Afterwards, a set of plane creation, 2D geometry sketching and “extrude cut material” function was performed to 3D sketch the orifice of the U-OWC chamber. The process is illustrated in Figure 3.16.

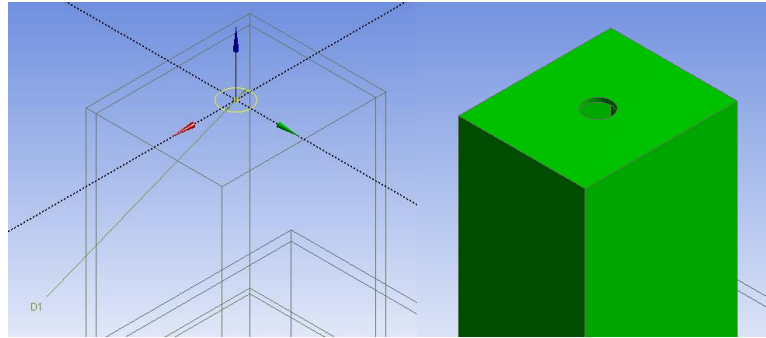


Figure 3.16: 3D Sketches of the Chamber Orifice

3.4.1.6 Fill Function

Lastly, “fill” function was performed to create air volume in the non-water-immersed chamber part. The setting of the function requires the user to select six inner faces of the non-water-immersed chamber part in order to create the air volume as shown in Figure 3.17.

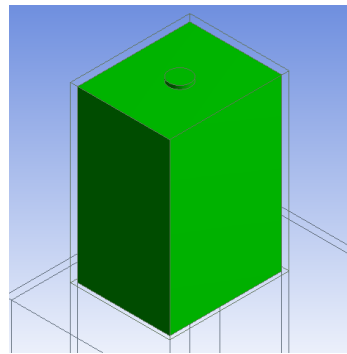


Figure 3.17: 3D View of the Air Volume

3.4.1.7 Overall View of the 3D Model

Self-defined name were set for the four 3D model parts to make an inspection on the correctness of the U-OWC sketches, for which the software confirmed that the 3D model sketched was comprised of 4 parts and 4 bodies as illustrated in Figure 3.18. The particular volume for each parts are shown in Figure 3.19 (Water), Figure 3.20 (TankWall), Figure 3.21 (UpperChamber) and Figure 3.22 (Air) correspondingly.



Figure 3.18: Components of the 3D Model

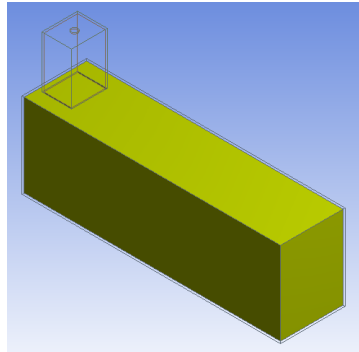


Figure 3.19: "Water" Part

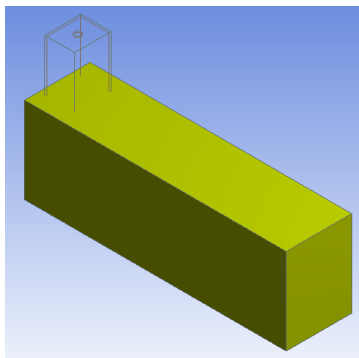


Figure 3.20: "TankWall" Part

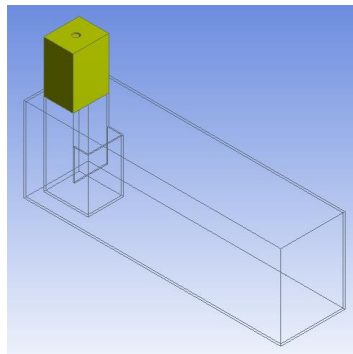


Figure 3.21: "UpperChamber" Part

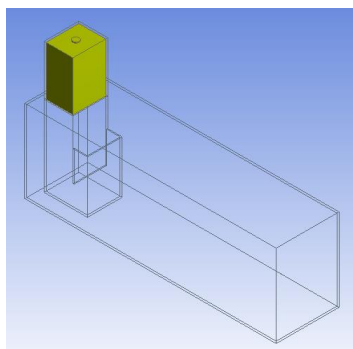


Figure 3.22: "Air" Part

3.4.2 Meshing

In this process, the 3D model was imported into the mesh solver, and hence the default mesh generation was performed by the mesh solver and the meshed 3D model is shown in Figure 3.23. Setting of mesh is crucial for the simulation results as the greater the mesh resolution, the higher the result accuracy. High mesh setting results long computing time that acquires computer with great processor and high computer memory. However, due to the specification limitations of the project computer (referred to Chapter 5.4), the appropriate mesh setup that has been selected for this project is shown in Figure 3.24. Remarkably, the minimum and the maximum mesh sizes were set as 0.00022 m and 0.022 m respectively. The chosen mesh settings are applied to all four U-OWC 3D models and the number of nodes and elements for every model are listed in Table 3.2.

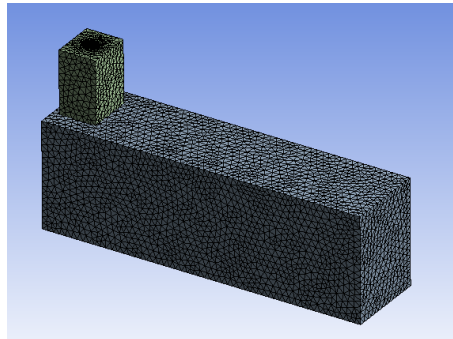


Figure 3.23: Meshed 3D Model

Details of "Mesh"	
⊕	Display
⊕	Defaults
⊖	Sizing
	Size Function Curvature
	Relevance Center Coarse
	Initial Size Seed Active Assembly
	Smoothing Medium
	Transition Slow
	Span Angle Center Fine
<input type="checkbox"/>	Curvature Normal A... Default (18.0 °)
<input type="checkbox"/>	Min Size 2.2e-004 m
<input type="checkbox"/>	Max Face Size 2.2e-002 m
<input type="checkbox"/>	Max Tet Size Default (0.138420 m)
<input type="checkbox"/>	Growth Rate Default (1.20)
	Automatic Mesh Base... On
<input type="checkbox"/>	Defeaturing Tolera... Default (1.1e-004 m)
	Minimum Edge Length 5.e-003 m

Figure 3.24: Mesh Settings

Table 3.2: Number of Nodes and Elements for the Four U-OWC 3D Models

Bottom Profile	Number of Nodes	Number of Elements
Flat	28039	118180
Circular	27917	117685
1:1 Slope	27836	117525
1:5 Slope	28076	117685

3.4.3 Setup

This sub-chapter presents the most critical part for the simulation, for which the settings of fluid domains, boundary conditions and initial conditions were set. The setup was started with the settings of “Analysis Type”, transient analysis was selected because the water wave movement was reliant on the time. The total simulation time and time step interval were set to 12 s and 0.1 s respectively as shown in Figure 3.25. Therefore, the total number of time step for the simulation was 120. Additionally, it was important to note that the settings of simulation time and time step interval were finalized after the occurrence of several times of simulation error which was termed as “Overflow in Linear Solver”. The detail explanation of this error is presented in Chapter 5.2.3.

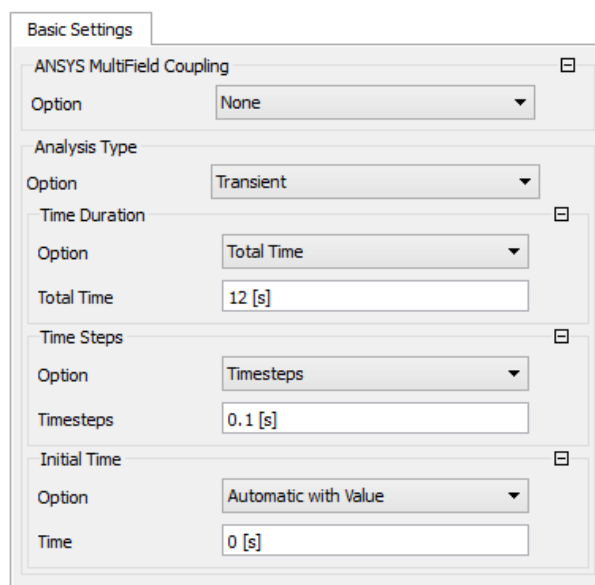


Figure 3.25: Settings of Analysis Type

3.4.3.1 Settings of Self-defined Expressions

Figure 3.26 shows the settings of ten self-defined expressions for the simulation. The expressions of “D”, “FluidD”, “H”, “L”, “P” and “WathH” are the fluid-related properties which are termed as the wave height, fluid density, water tank height, wavelength, wave period and water depth correspondingly.

Whereas the expressions of “HydroSP”, “WatVF”, “Vx” and “Vy” are named as hydrostatic pressure, water volume fraction, horizontal wave function and vertical wave function respectively. The purpose of these four expressions was to generate water wave motions.

Expression Name	Value / Formula
D	0.1[m]
FluidD	998[kg m ⁻³]
H	0.5[m]
HydroSP	FluidD*g*(WathH-y)*WatVF
L	5.5[m]
P	1[s]
Vx	$(\pi/(2*P))*H*e^{((-2*\pi*D)/L)}*\cos(2*\pi*((x/L)-(t/P)))$
Vy	$(\pi/(2*P))*H*e^{((-2*\pi*D)/L)}*\sin(2*\pi*((x/L)-(t/P)))$
WathH	0.4[m]
WatVF	if(y<=WathH,1,0)

Figure 3.26: Self-defined Expressions

3.4.3.2 Settings of Water and Air Domain

Water domain and air domain were inserted to the flow analysis, Figure 3.27 shows the locations for the water domain and air domain respectively. The “basic settings” and “fluid models” settings were the same for both water domain and air domain but the only difference setting was the “initialization”.

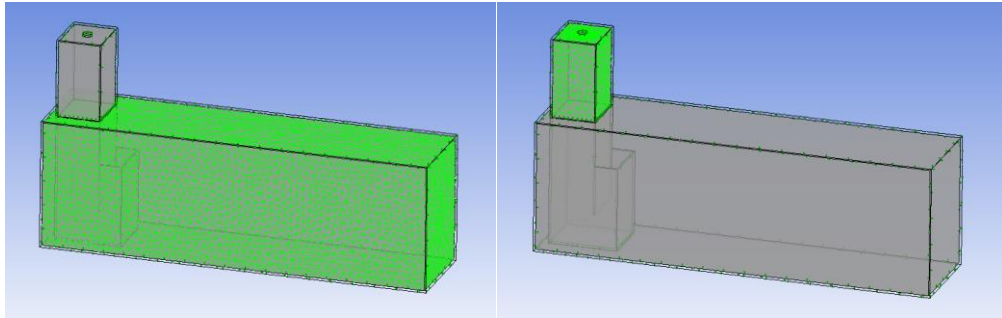


Figure 3.27: Water Domain (Left) and Air Domain (Right)

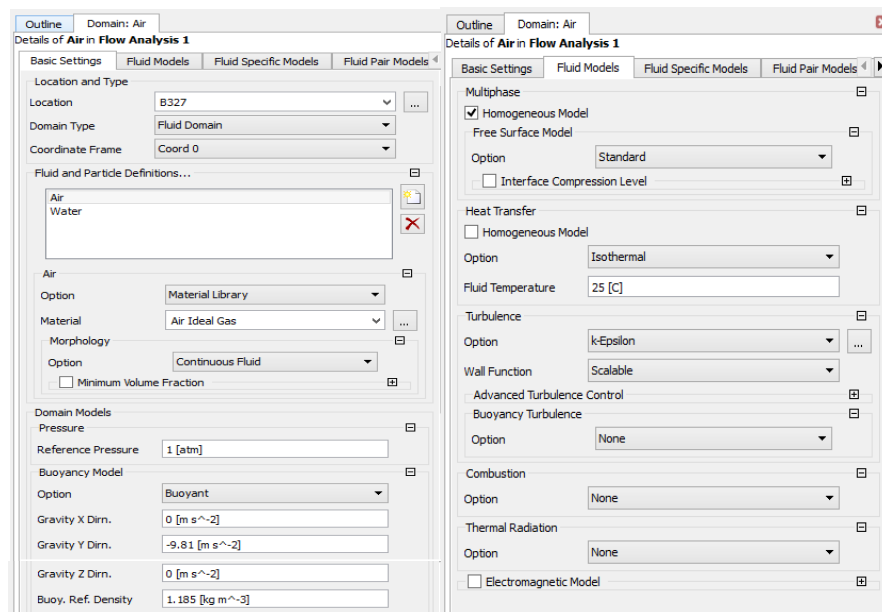


Figure 3.28: Domain Basic Settings (Left) and Domain Fluid Models (Right)

Under the tab of “basic Settings - fluid and particle definitions”, air was set as air ideal gas and water was set as water. At the tab of “basic settings - buoyancy model”, the gravity effect was created by setting the Y gravity direction as -9.81 ms^{-2} and the buoyancy reference density was set to 1.185 kgm^{-3} in order to turn on the buoyancy effect.

Next, “homogenous model” function was turned on under the tab of “Fluid Models-Multiphase” because the flows of air and water in the U-OWC were assumed to be in the same direction. The explained settings are shown in Figure 3.28.

Figure 3.29 and Figure 3.30 shows the “initialization” settings for the air domain and water domain respectively. For air domain and water domain, the “domain initialization” function was turned on and the values of “cartesian velocity components” were set to zero to simulate the zero motions of water and air at time

zero. Next, the “relative pressure” was set as 0 for air domain due to ambient pressure whereas HydroSP was set for water domain due to hydrostatic pressure that was exerted by water.

Furthermore, for the air domain, the “volume fraction” under the “fluid specific initialization” were set as 1 for air and 0 for water so that the air domain will only be filled by air at the time zero. Whereas for the water domain, the “volume fraction” under the “fluid specific initialization” was set as 1-WatVF for air and WatVF for water so that the water domain will be filled with water and air at the time zero.

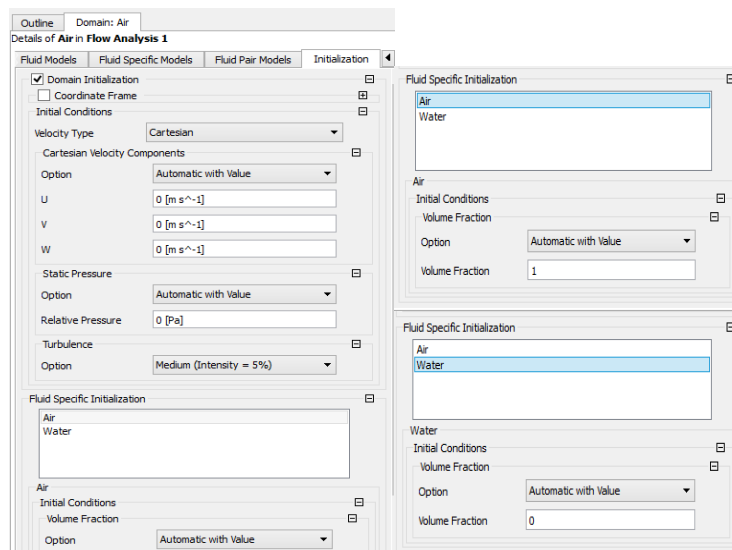


Figure 3.29: Initialization Settings of Air Domain

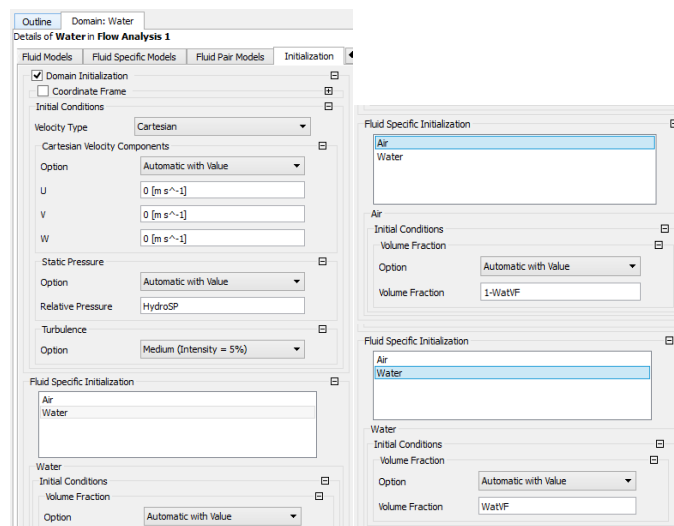


Figure 3.30: Initialization Settings of Water Domain

3.4.3.3 Settings of Boundary Conditions for Water Domain

Three boundary conditions were set for the water domain namely, wall, inlet and opening. The purpose of setting the wall boundary condition was to let the software to recognize the water-immersed chamber walls. The locations of the wall boundary are shown in the Figure 3.31. Only two settings were required for the wall boundary which were the selection of “wall” under the “boundary type” and “no slip wall” under the “boundary detail”. The settings are demonstrated in Figure 3.32.

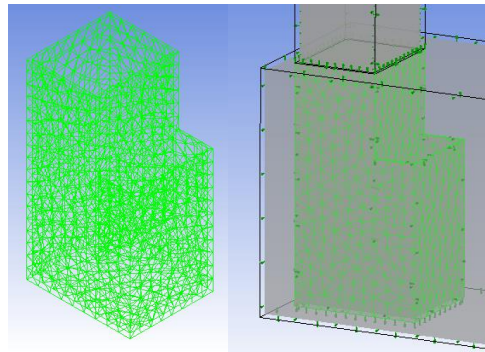


Figure 3.31: Location of Wall Boundary Condition of Water Domain

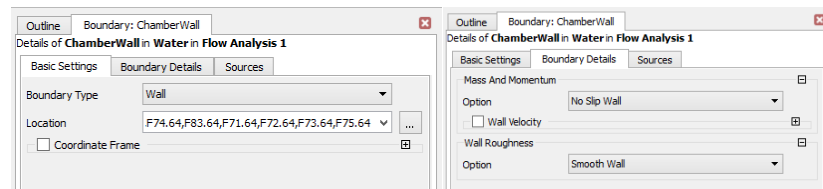


Figure 3.32: Settings for Wall Boundary Condition for Water Domain

The second boundary condition for water domain was the inlet. The setting of inlet boundary condition was set to indicate the input for the water wave. Location of the inlet boundary is shown in Figure 3.33. Under the tab of “boundary details - cartesian velocity components”, wave functions of V_x and V_y were set as the U value and V value respectively whereas 0 was set for the W value because it was assumed that there was no velocity across the width of the water tank. Under the tab of “fluid values - volume fraction”, 1-WatVF was set for air and WatVF was set for water. The corresponding settings are illustrated in Figure 3.34.

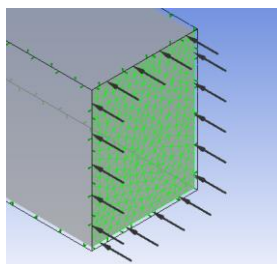


Figure 3.33: Location of Inlet Boundary Condition of Water Domain

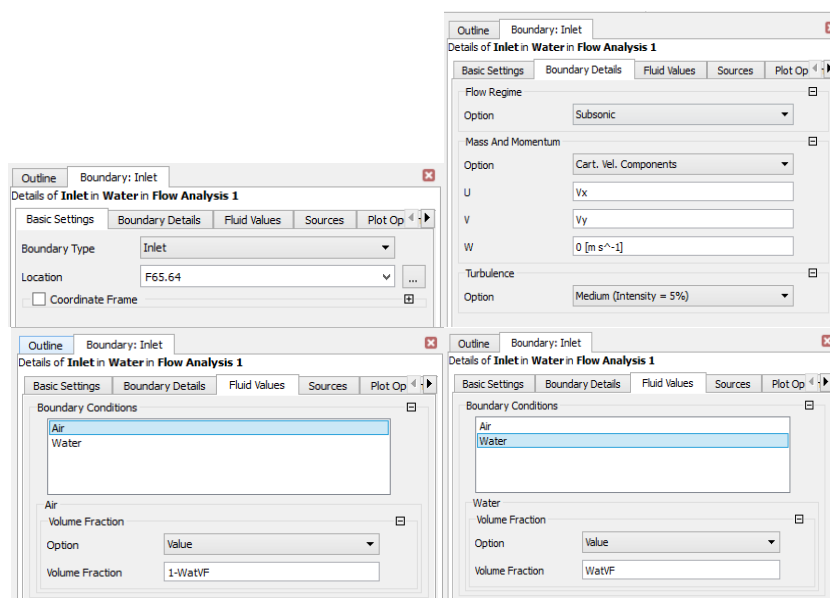


Figure 3.34: Settings of Inlet Boundary Condition of Water Domain

The third boundary condition for water domain was the opening. The setting of opening boundary condition was to simulate the opening of tank wall. Location of the opening boundary is shown in Figure 3.35 and Figure 3.36. Under the tab of “boundary details - mass and momentum - opening pressure and direction”, the relative pressure of 0 was set. Under the tab of “fluid values - volume fraction”, 1 was set for air and 0 was set for water. The corresponding settings are illustrated in Figure 3.37.

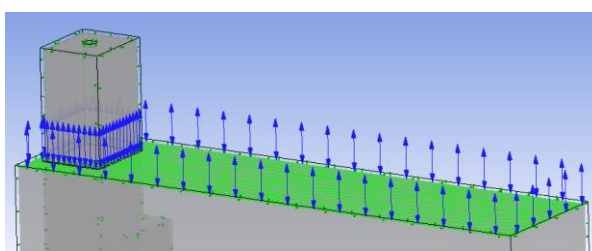


Figure 3.35: Location of Opening Boundary Condition of Water Domain

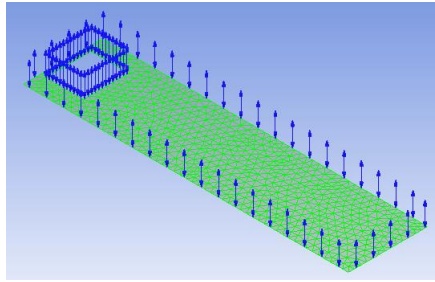


Figure 3.36: Detail View of the Opening Boundary Condition of Water Domain

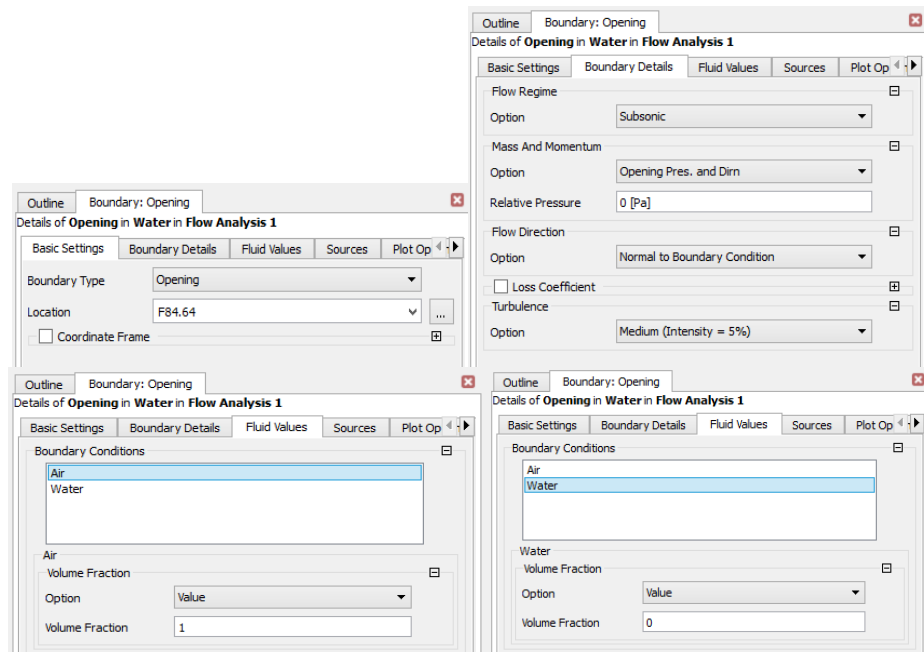


Figure 3.37: Settings of Opening Boundary Condition of Water Domain

3.4.3.4 Settings of Boundary Conditions for Air Domain

There was only one boundary condition for the air domain which was the opening. The setting of opening boundary condition was to allow the air to flow in and out from the U-OWC chamber. Location of the opening boundary is shown in Figure 3.38. Under the tab of “boundary details - mass and momentum - opening pressure and direction”, the relative pressure of 0 was set. Under the tab of “fluid values - volume fraction”, 1 was set for air and 0 was set for water. The corresponding settings are shown in Figure 3.39.

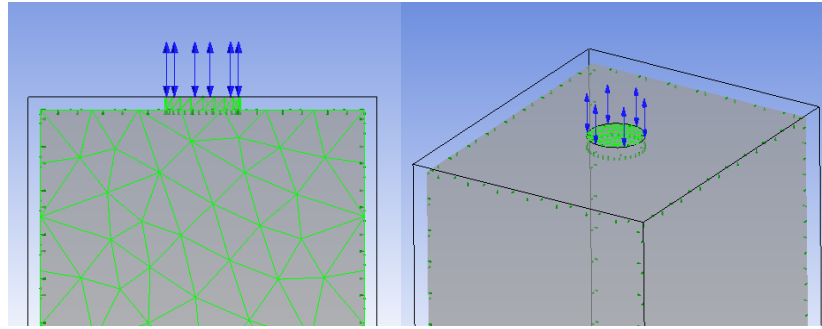


Figure 3.38: Location of Opening Boundary Condition of Air Domain

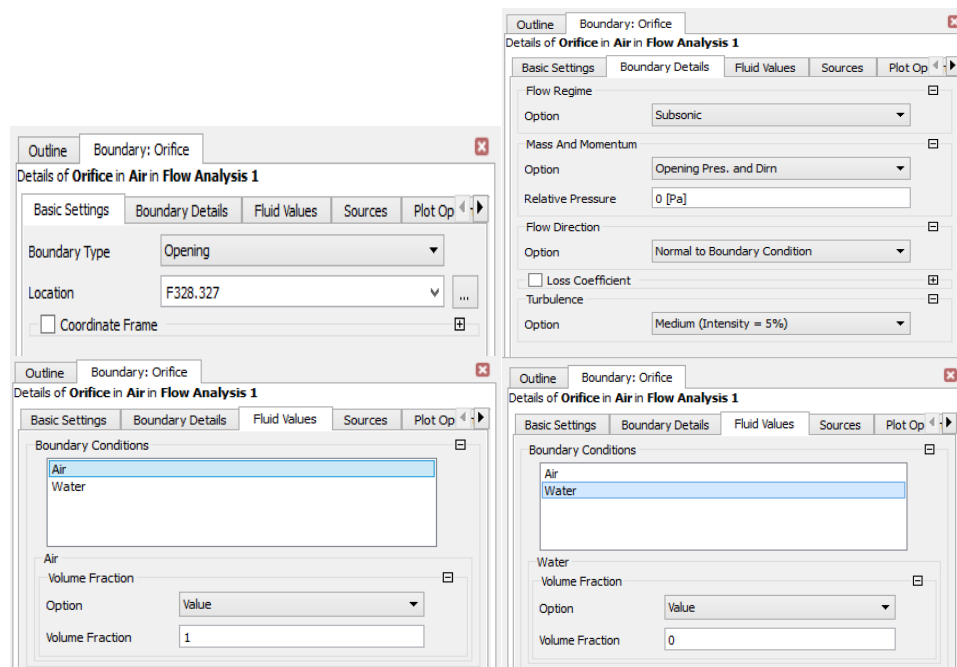


Figure 3.39: Settings of Opening Boundary Condition of Air Domain

3.4.4 Solution Generation

Under the tab of “run definition - run settings”, “double precision” was selected and the “platform MPI local parallel” was set for the run mode. Furthermore, the “partitions” was set as 4 because the number of processor cores for the project computer was 4. The respective settings are shown in Figure 3.40. Afterwards, the “start run” was clicked to run the simulation. Figure 3.41 illustrates the simulation run process.

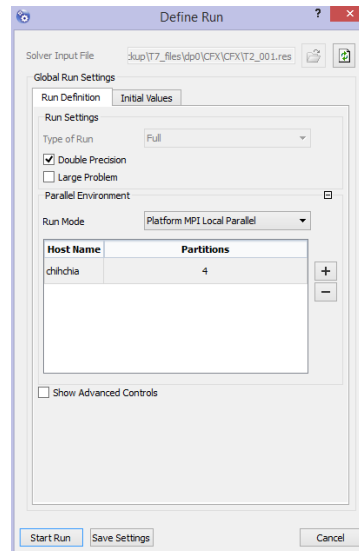


Figure 3.40: Define of Run Settings

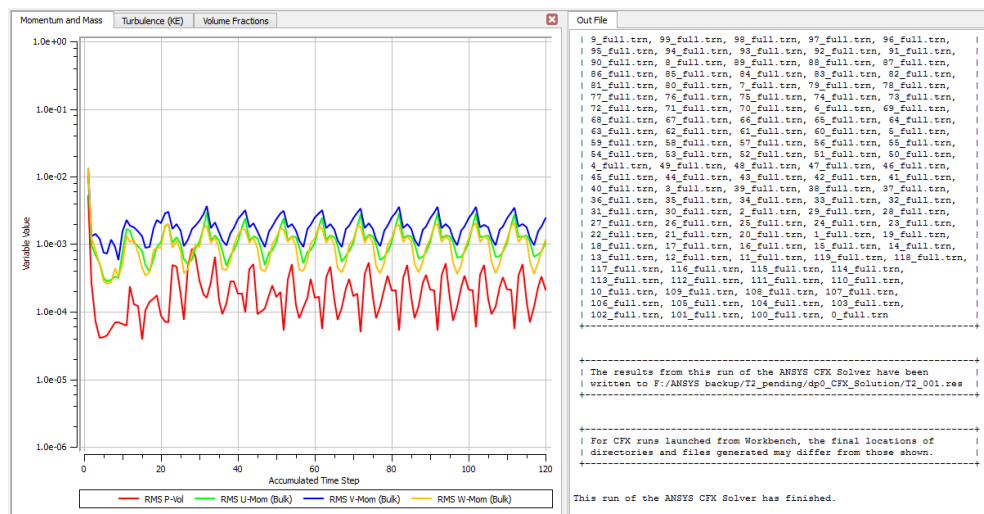


Figure 3.41: Run of Simulation

3.4.5 CFD-Post

After the completion of the simulation run, the simulation results were stored in the CFD-Post and the simulation results were visualized by the “plot” functions. Under the tab of “outline - user locations and plot”, there were several types of useful plot that can be inserted into the simulated 3D model as shown in Figure 3.42.

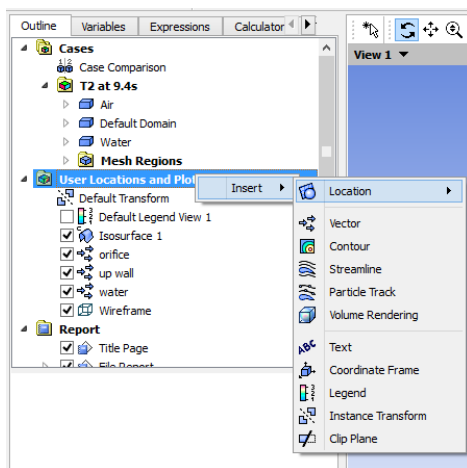


Figure 3.42: Choices of Plot

Isosurface plot was set to visualize the motion of the water surface in the water tank. Under the “Geometry” tab, “Water.Volume Fraction”, “Hybrid” and value of 0.5 was set. Figure 3.43 shows the settings of Isosurface and the effect of Isosurface plot.

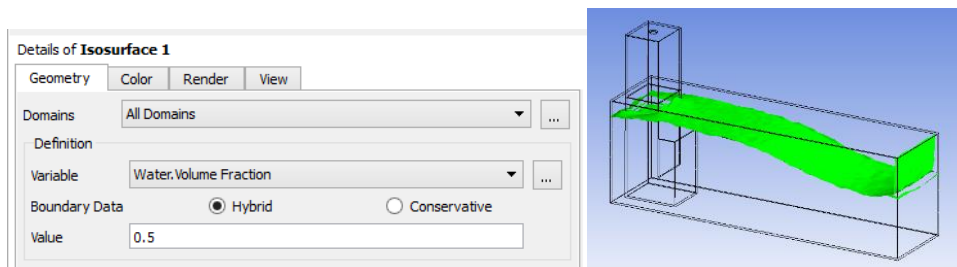


Figure 3.43: Settings of Isosurface Plot (Left) and Isosurface Plot (Right)

In order to observe the chamber “inhalation” and “exhalation” mechanisms, Vector plot was used. Under the “Geometry” tab, “orifice” was selected as the “location” and the “air.superficial velocity” was set as “variable”. The corresponding settings and the air Vector plot effect are shown in Figure 3.44.

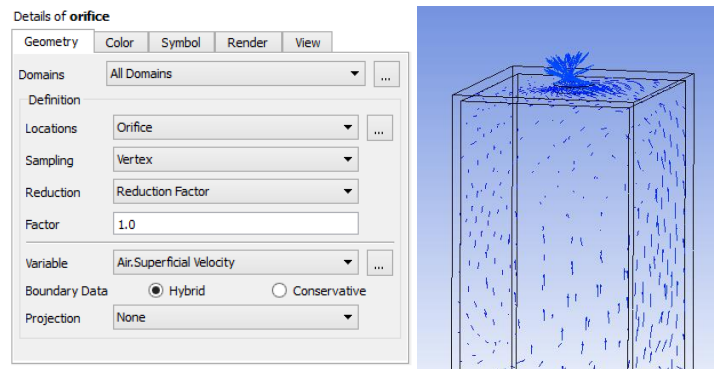


Figure 3.44: Settings of Air Vector Plot (Left) and Air Vector Plot (Right)

Moreover, Vector plot was used to observe the water wave inner mechanisms. Under the “Geometry” tab, “water” was selected as the “location” and the “water.superficial velocity” was set as “variable”. The corresponding settings and the water Vector plot effect are shown in Figure 3.45.

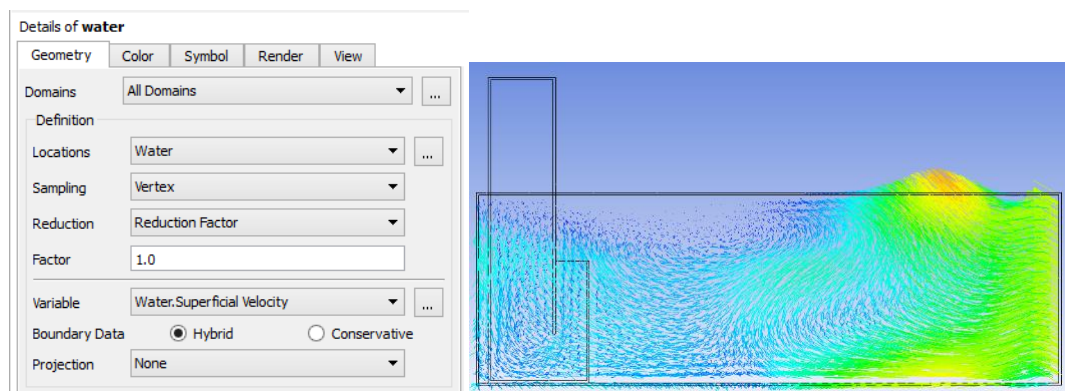


Figure 3.45: Settings of Water Vector Plot (Left) and Water Vector Plot (Right)

After setting up the desired plots, Animation function was used to animate the water waves. The setting for the Animation function was “timestep animation” as displayed in Figure 3.46. Figure 3.47 show the screenshots of animation of the Flat Bottom Profile U-OWC and the Circular Bottom Profile U-OWC whereas Figure 3.48 illustrate the screenshots of animation of the 1:1 Slope Bottom Profile U-OWC and the 1:5 Slope Bottom Profile U-OWC.

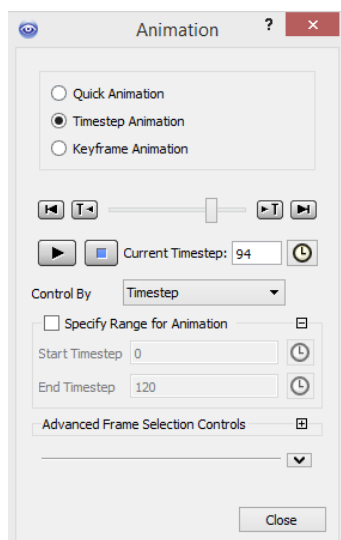


Figure 3.46: Animation Function for the Simulated 3D Model

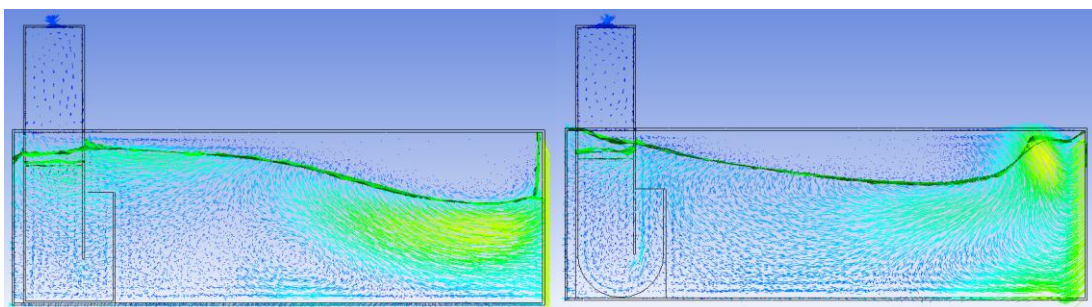


Figure 3.47: Plotted Results of Flat Bottom Profile U-OWC (Left) and Circular Bottom Profile U-OWC (Right)

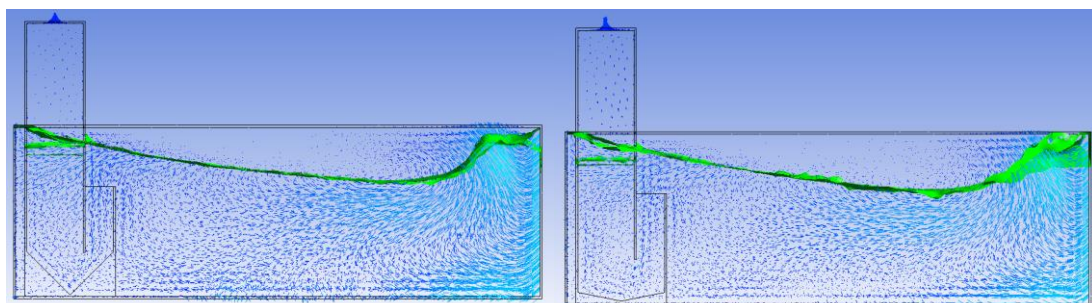


Figure 3.48: Plotted Results of 1:1 Slope Bottom Profile U-OWC (Left) and 1:5 Slope Bottom Profile U-OWC (Right)

3.4.5.1 Function Calculator

The average air velocity and the average air pressure were calculated by the Function Calculator. To calculate the average air velocity, the “areaAve” was selected as

“function”, “orifice” was selected as the “location”, “air.superficial velocity” was chosen as the “variable” and the “calculate” was clicked. Same settings were performed to calculate the average air pressure, except that the “default fluid fluid interfase in air side 1” was chosen as the “location”.

The Function Calculator was able to show the function expression by turning on the setting of “show equivalent expression”. The expressions were copied (as shown in Figure 3.50) and pasted into the “expression” library for the use of graph plotting. The newly created expressions are shown in Figure 3.51.

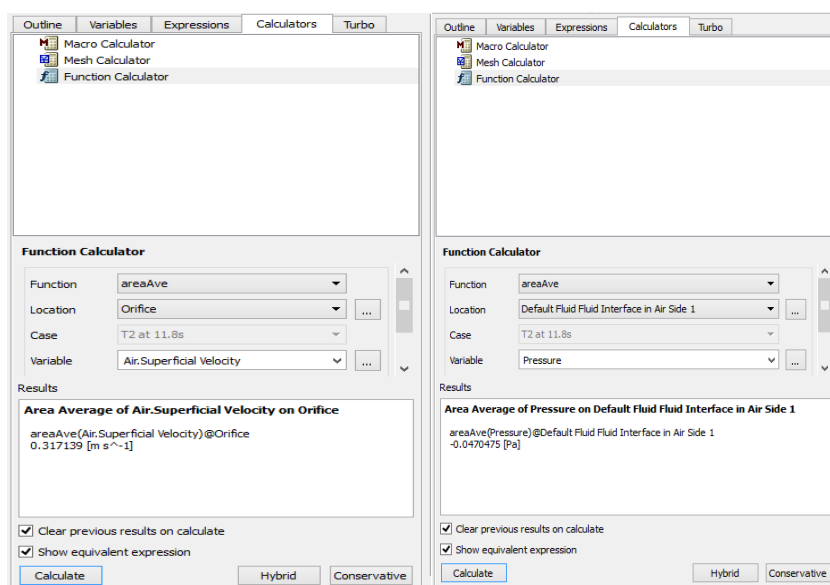


Figure 3.49: Function Calculators of Air Velocity (Left) and Air Pressure (Right)

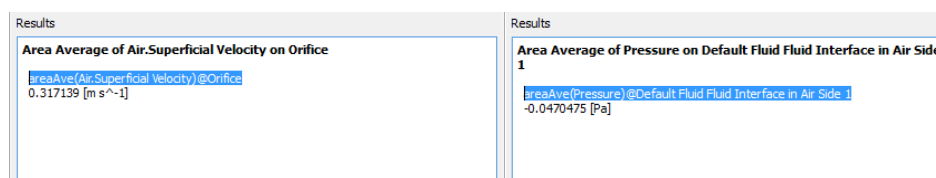


Figure 3.50: Equations of Average Air Velocity (Left) and Average Air Pressure (Right)

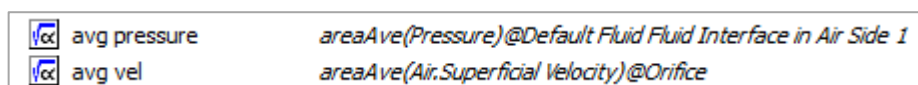


Figure 3.51: Self-defined Expressions

3.4.5.2 Graphs Plotting

The values of the average air velocity and average air pressure were plotted against the time steps by performing the Chart function. The important settings for the Chart function are shown in Figure 3.52 and Figure 3.53. Figure 3.54 shows an example of graph of average air velocity against the accumulated time step.

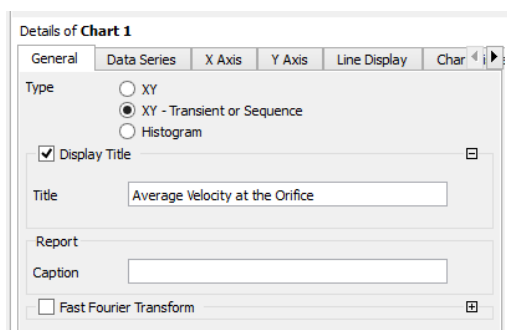


Figure 3.52: Chart Function Settings Part 1

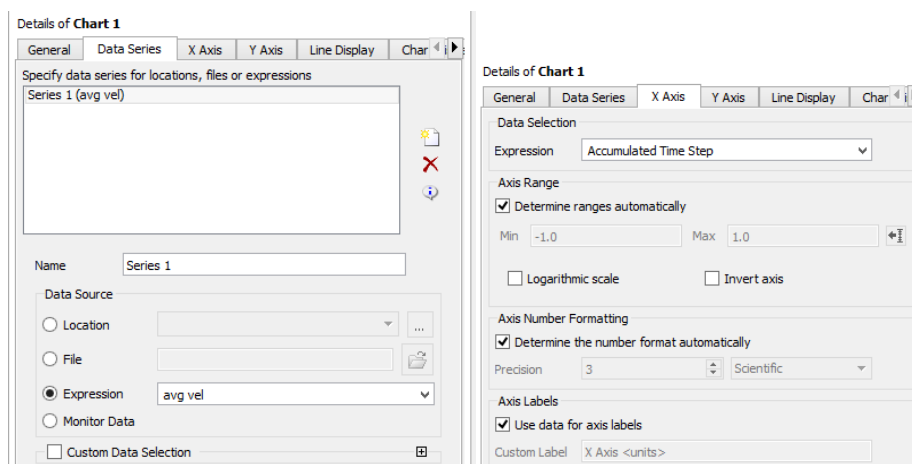


Figure 3.53: Chart Function Settings Part 2 (Left) and Chart Function Settings Part 3 (Right)

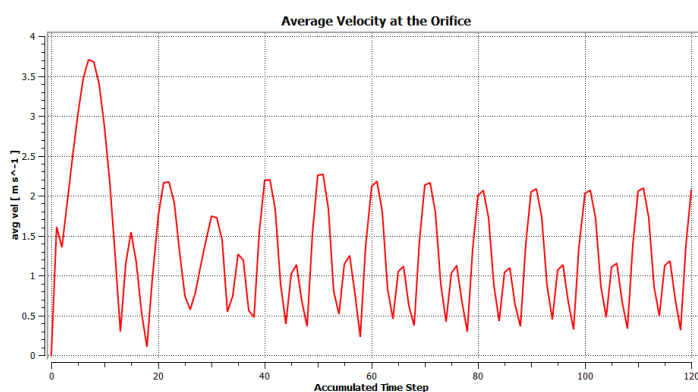


Figure 3.54: Sample Air Velocity Graph

In order to obtain all the calculated results with respect to the 120 time steps in the terms of average air velocity and average air pressure, “export” function was used to generate the Microsoft Excel files that comprised the complete sets of average air velocity values and average air pressure values. Subsequently, the excel data will be used for result analysis and discussion. Appendix A and Appendix B contain the simulated results of average air velocity and average air pressure respectively.

3.5 Experimental Phase

After the completion of result analysis and discussion as explained in Chapter 4.2, U-OWC with circular bottom profile as illustrated in Figure 3.55 was found to be the optimum design that generated the ultimate air-discharge velocity, the highest air-discharge pressure and the greatest power output. Thereafter, the prototype was built according to the simulated U-OWC dimensions to verify the simulation results. Based on the overall view of the prototype as shown in Figure 3.56, it is observed that it consists of five major components:

- i. Water tank
- ii. U-OWC chamber with circular bottom profile
- iii. Enhancement frames of water tank walls
- iv. Arduino water wave generator
- v. Arduino pressure sensor

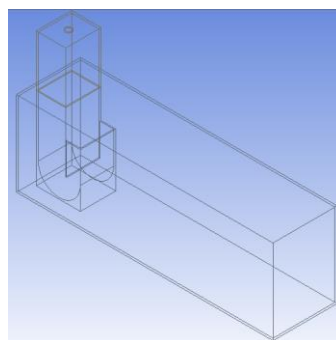


Figure 3.55: Isometric View of 3D Sketch of Circular Bottom Profile U-OWC



Figure 3.56: Overall View of the Prototype

3.5.1 Water Tank

The water tank as shown in Figure 3.57 was retrieved from the former FYP project. Silicone Glue as shown in Figure 3.58 was re-applied to the bottom wall sides and wall corners to ensure no water leakage during the experiment.



Figure 3.57: Water Tank



Figure 3.58: Silicone Glue

3.5.2 U-OWC Chamber with Circular Bottom Profile

The circular bottom profile was fabricated based on the dimensions of the circular bottom profile as shown in Chapter 3.3.2 with the material of 0.2 mm aluminium sheet. Due to the extreme thin of sheet thickness, the aluminium sheet was folded to create the double-layered thickness. Faber-Castell sticky plasticine as shown in Figure 3.59 (Left) was used to hold the position of circular bottom profile inside the

U-OWC chamber according to the simulated position. Figure 3.59 (Right) illustrates one of the adhesive layers of the circular bottom profile and Figure 3.60 displays the overview of the U-OWC chamber with circular bottom profile.



Figure 3.59: Faber-Castell Plasticine (Left) and Adhesive Layer of the Circular Bottom Profile (Right)

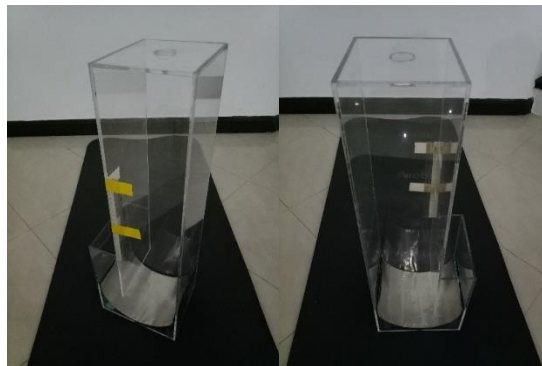


Figure 3.60: U-OWC Chamber with Circular Bottom Profile

3.5.3 Enhancement Frames for Water Tank Walls

A set of metal frames as shown in Figure 3.61 were fabricated and installed around the “weak” sections of the water tank. The “weak” sections are referred to the long side walls which could not withstand the high water pressure and caused bending effect to the tank walls during the experiment. Detail explanation on the tank wall bending problem is discussed in Chapter 5.3.1. With the supports of the metal frames, the mechanical strength of the water tank walls was enhanced and the breakage of tank side walls was avoided.



Figure 3.61: Steel Enhancement Frames

3.5.4 Arduino Water Wave Generator

Arduino water wave generator as demonstrated in Figure 3.62 was constructed to generate the consistent water waves that were similar to the simulated water waves. Specifically, the water wave generator was composed of an Arduino microcontroller, two servo motors and a pair of paddles. The construction steps of water wave generator are summarized as:

1. Coding was programmed into the servo motors with the Arduino circuits.
2. Linkages of the servo motors were fabricated and attached at the arms of the servo motor.
3. Paddles were fabricated and pivoted on the bottom of water tank.
4. Connections between the paddles and servo motors arm-linkages were established.
5. 5 V electrical input was supplied for the Arduino circuit to operate the water wave generator through USB cable.
6. Paddles were controlled by the servo motors to perform back-and-forth motions.
7. Water waves were generated.



Figure 3.62: Overview of Arduino Water Wave Generator

3.5.4.1 Circuit Diagram of the Servo Motors

Coding for the servo motors is attached in Appendix G. Figure 3.63 shows the circuit connections for the servo motors. In the circuit, a 100 k Ω adjustable rotary resistor was installed to control the speed of the servo motors in terms of servo motor response time, in precise, the response time was finalized as 690 ms after several trials because with the 690 ms response time, the experimental average air-discharge velocity was found to be the highest. Detail information about the response time setting can be referred to Appendix G.

Furthermore, a normally-open switch was installed to initiate or to pause the Arduino water wave generator and a 16 k Ω resistor was included to stabilize the electrical signal of the normally-open switch. It was important not to ignore that the servo motors were connected to the “5 V” port but not the “3.3 V” port of the Arduino board so that the servo motors could acquire the sufficient electrical supply to move the paddles in the water-immersed condition or so called the high water pressure condition. Figure 3.64 shows the actual view of the circuit connection of the servo motors.

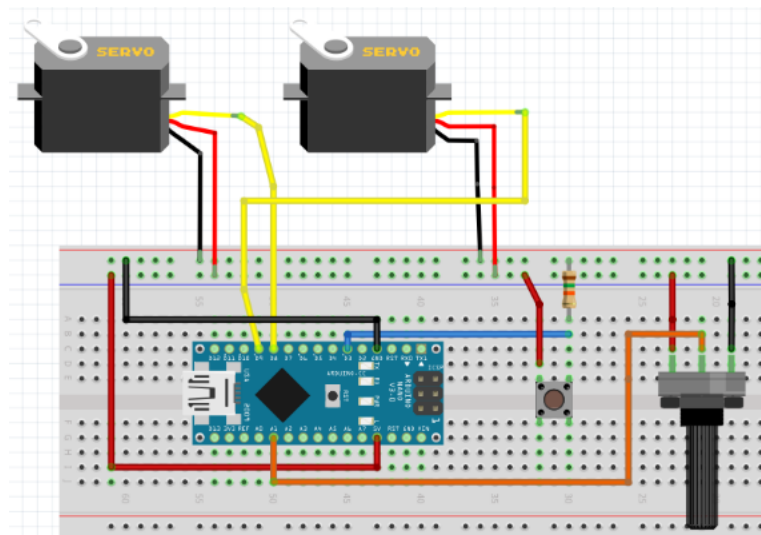


Figure 3.63: Circuit Diagram of Servo Motors

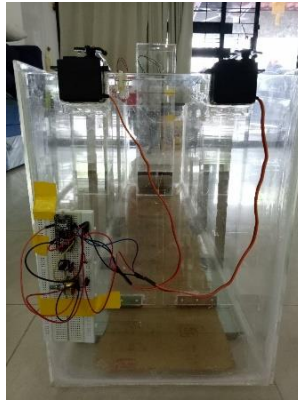


Figure 3.64: View of Circuit Connection of Servo Motors

3.5.4.2 Servo Motor Arm-linkage

The purpose of servo motor arm-linkage was to convert the rotational force produced by the servo motor into compressive force which was used to push and to pull the paddles and hence producing the water waves. A set of the servo motor arm-linkage was composed of a 2 mm metal string and 2 acrylic bars. The two acrylic bars were hot glued to the servo motor tip and the paddle top region respectively whereas the metal string was the link between the paddle and the servo motor. Figure 3.65 shows the detail views of the servo motor arm-linkage.



Figure 3.65: Detail Views of Servo Motor Arm-linkages

3.5.4.3 Paddle

Figure 3.66 shows the image of paddles of the water wave generator. The paddles were made up of 2 pieces of 2 mm Acrylic sheets. In order to create the pivot points for the paddles that could enable the back-and-forth motion, a door hinge was attached at the bottom of each acrylic sheet with the adhesive of hot glue.



Figure 3.66: Paddles of Arduino Water Wave Generators

3.5.5 Arduino Pressure Sensor

Arduino pressure sensor as shown in Figure 3.67 was used to measure the air-discharge pressure at the chamber orifice. Precisely, the water wave generator was composed of an Arduino microcontroller and a barometric pressure sensor (BME280). To establish the pressure sensor, coding was programmed into the BME280 pressure sensor and then the electrical supply of 3.3 V was supplied with USB cable for the Arduino microcontroller to operate the pressure sensor. Figure 3.68 displays the circuit diagram of Arduino pressure sensor and the coding of Arduino pressure sensor is attached in Appendix H.

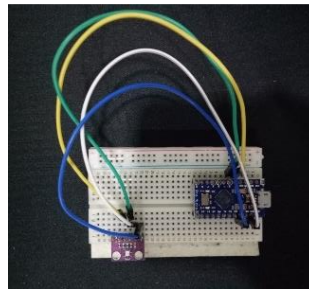


Figure 3.67: View of Circuit Connection of Pressure Sensor

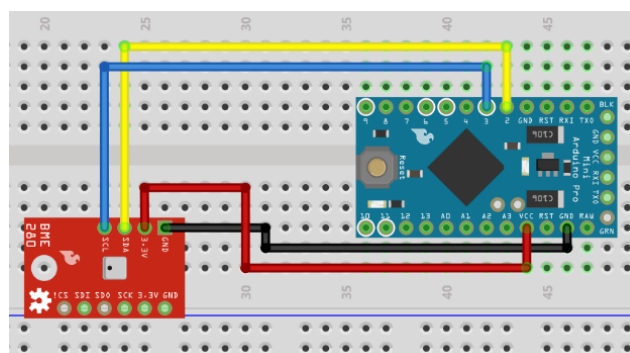


Figure 3.68: Circuit Diagram of Pressure Sensor

3.5.6 Experiment Setup

Figure 3.69 illustrates the view of experiment setup. For mechanical parts, the U-OWC chamber was placed in the water tank according to the simulated position. U-OWC final assembly was filled with water until the marked level which was defined according to the simulated chamber immersion depth. Enhancement frames were installed on the side walls of the water tank. Whereas for electronic parts, Arduino boards of the water wave generator and pressure sensor were electrically supplied by the USB cables.



Figure 3.69: Experiment Setup

3.5.6.1 Collection of Experimental Results

Digital vane anemometer as shown in Figure 3.70 (Left) was used to measure the air-discharge velocity and the Arduino pressure sensor as shown in Figure 3.70 (Right) was used to measure the air-discharge pressure. Both measurements were performed on the parallel top surface of the chamber orifice which was about 1 cm in distance.



Figure 3.70: Digital Vane Anemometer (Left) and Arduino Pressure Sensor (Right)

3.5.6.2 Experiment Procedure

The experimental steps are conducted as following,

1. Adjustable resistor knob of Arduino water wave generator was adjusted to “690 ms”.
2. Normally-open switch of the Arduino water wave generator was pressed for 2 s to activate the wave generator.
3. Water waves were generated by the back-and-forth motions of the paddles.
4. Digital vane anemometer was held on the orifice surface of the U-OWC chamber.
5. The air-discharge velocity was displayed by the anemometer and the result was recorded.
6. Step (4) to step (5) were repeated for 18 s.
7. Arduino pressure sensor was held on the orifice surface of the U-OWC chamber.
8. The air-discharge pressure was displayed on the screen of Arduino Program and the result was recorded.
9. Step (7) to step (8) were repeated for 18 s.
10. Normally-open switch of the Arduino water wave generator was pressed for 2 s to stop the Arduino water wave generator.
11. The experimental results were plucked into Microsoft Excel worksheet for evaluation and discussion.

Experimental results of air-discharge velocity are shown in Appendix C. Screenshots of the experimental results of air-discharge pressure are shown in Appendix D. Experimental results of air-discharge pressure are shown in Appendix E.

CHAPTER 4

RESULTS AND DISCUSSIONS

4.1 Introduction

The simulation results which are in terms of air velocity and air pressure were obtained from the ANSYS CFX 17 software simulation while the experimental results were collected by digital anemometer for air velocity and Arduino barometric pressure sensor BME280 for air pressure.

4.2 Simulation Results

This sub-chapter presents the simulation results of the four U-OWC models.

4.2.1 Flat Bottom Profile U-OWC

Figure 4.1 shows the air velocity graph of the flat bottom profile U-OWC while Figure 4.2 shows the air pressure graph of the flat bottom profile U-OWC. Based on Figure 4.1, it is observed that the trend line shows a very unstable change at the early stage and then followed by the consistent state. The behaviour of trend line specifies that the simulated air velocity values are undergoing the transient phase from time step of 0 to about time step of 40. This period of time steps can be explained as the water wave's build-up stage.

Whereas from the time step of 40 onwards, the trend line appears to be stable water waves that shows the consistency of chamber "inhalation" and chamber "exhalation", where such phase is termed as the stable state. The stable state can provide results with the minimal error due to its consistency and thus, it is worth examining more closely on the simulation results which fall in the range of stable state, particularly, ranging from time step of 40 to time step of 120.

On the other hand, the trend line in the Figure 4.2 shows the similar behaviour to the trend line in Figure 4.1, for which the pressure values vary drastically from time step of 0 to time step of 40 and then followed by stable state which happened from time step of 40 to time step of 120.

By only considering the stable state of the simulation results, it is determined that the air velocity values ranging from the lowest of 0.2293 ms^{-1} to the highest of

2.2693 ms^{-1} , whereas the air pressure values, ranging from the lowest of 0.0059 Pa to the highest of 2.9777 Pa . Note that the negative values for the air pressure are set to be absolute because the negative sign only indicates the flow of air pressure from ambient air into the chamber and does not affect the magnitude of the pressure value.

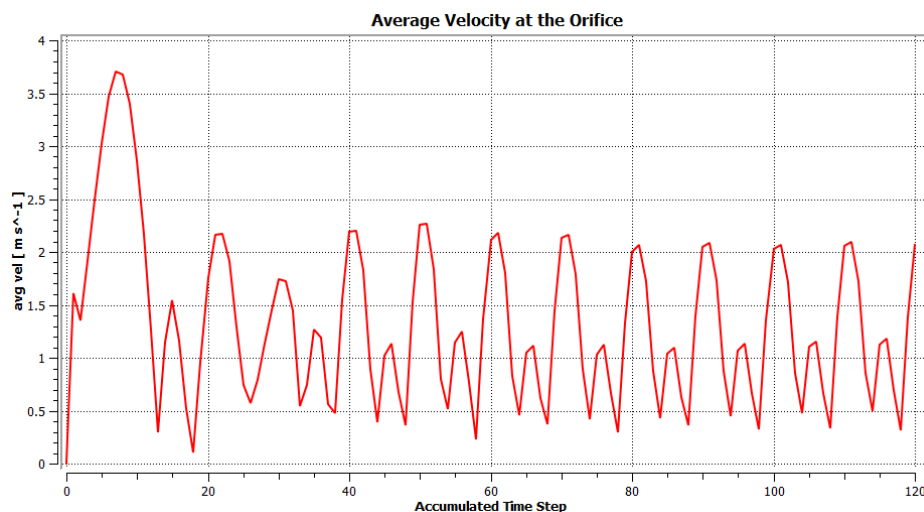


Figure 4.1: Air Velocity Graph of the Flat Bottom Profile U-OWC Chamber

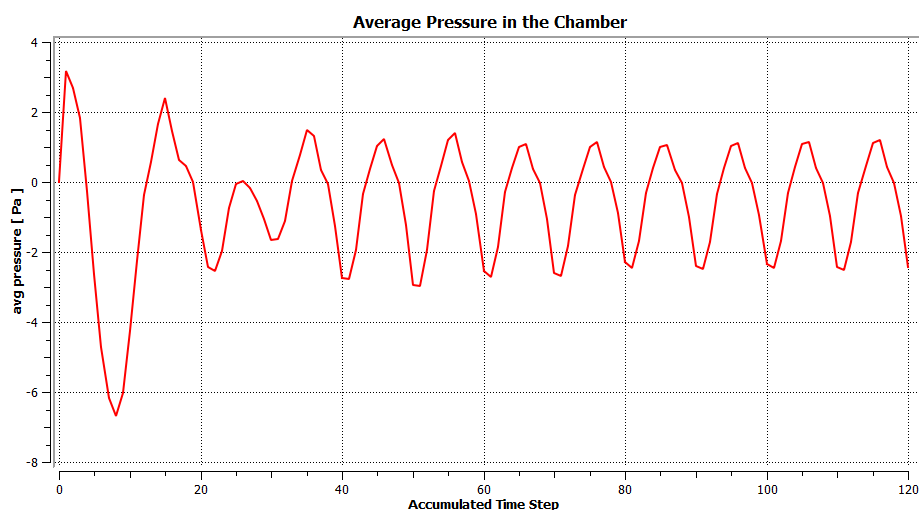


Figure 4.2: Air Pressure Graph of the Flat Bottom Profile U-OWC Chamber

4.2.2 Slope 1:1 Bottom Profile U-OWC

Figure 4.3 illustrates the air velocity graph of the slope 1:1 bottom profile U-OWC and Figure 4.4 illustrates the air pressure graph of the slope 1:1 bottom profile U-OWC. The trend lines in Figure 4.3 and Figure 4.4 behave similarly to the trend lines

4.2.3 Slope 1: 5 Bottom Profile U-OWC

Figure 4.5 displays the air velocity graph of the slope 1:5 bottom profile U-OWC and Figure 4.6 displays the air pressure graph of the slope 1:5 bottom profile U-OWC. The trend lines in Figure 4.5 and Figure 4.6 behave similarly to the trend lines produced by the flat bottom profile U-OWC, the detail explanation can be referred to Chapter 4.2.1.

By only considering the stable state of the simulation results, it is determined that the air velocity values ranging from the lowest of 0.1170 ms^{-1} to the highest of 2.9673 ms^{-1} , whereas the air pressure values, ranging from the lowest of 0.0006 Pa to the highest of 5.1642 Pa .

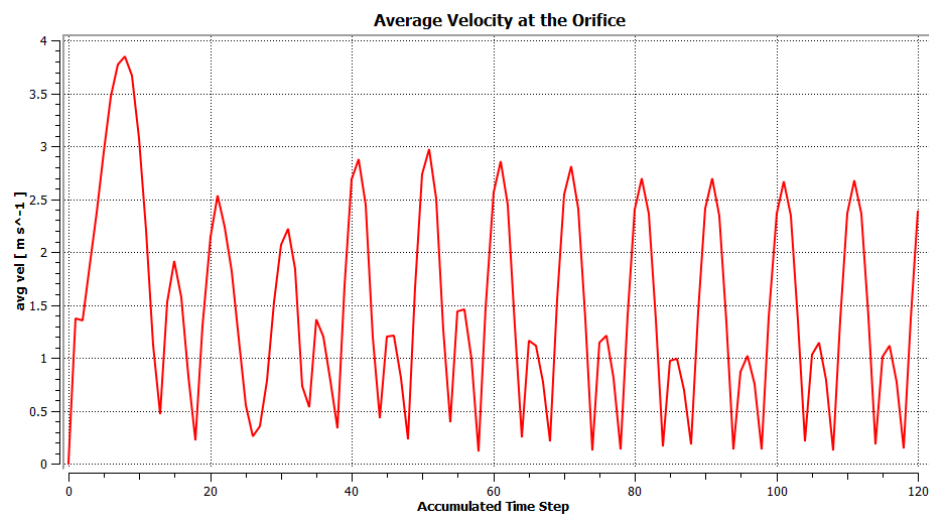


Figure 4.5: Air Velocity Graph of the 1:5 Slope Bottom Profile U-OWC Chamber

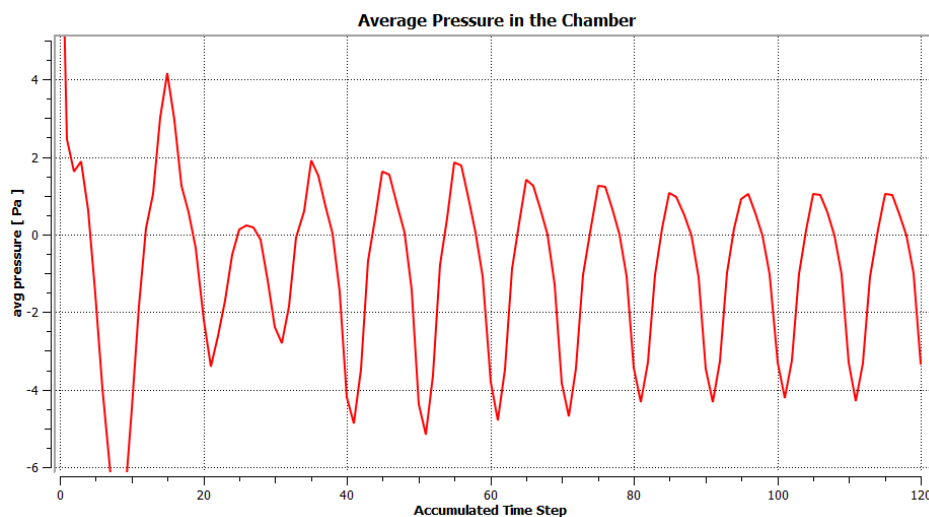


Figure 4.6: Air Pressure Graph of the 1:5 Slope Bottom Profile U-OWC Chamber

4.2.4 Circular Bottom Profile U-OWC

Figure 4.7 shows the air velocity graph of the circular bottom profile U-OWC and Figure 4.8 shows the air pressure graph of the circular bottom profile U-OWC. The trend lines in Figure 4.7 and Figure 4.8 behave similarly to the trend lines produced by the flat bottom profile U-OWC, the detail explanation can be referred to Chapter 4.2.1.

By only considering the stable state of the simulation results, it is determined that the air velocity values ranging from the lowest of 0.2730 ms^{-1} to the highest of 3.0892 ms^{-1} , whereas the air pressure values, ranging from the lowest of 0.1590 Pa to the highest of 4.7650 Pa .

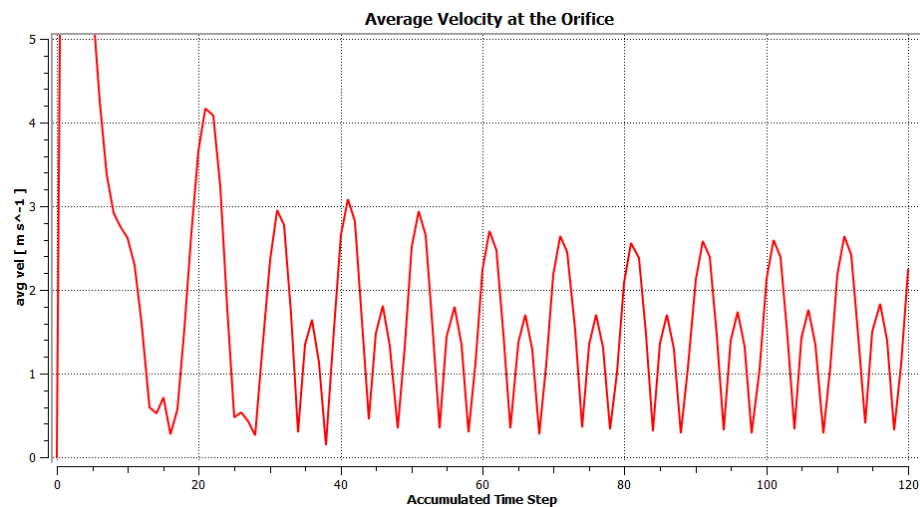


Figure 4.7: Air Velocity Graph of the Circular Bottom Profile U-OWC Chamber

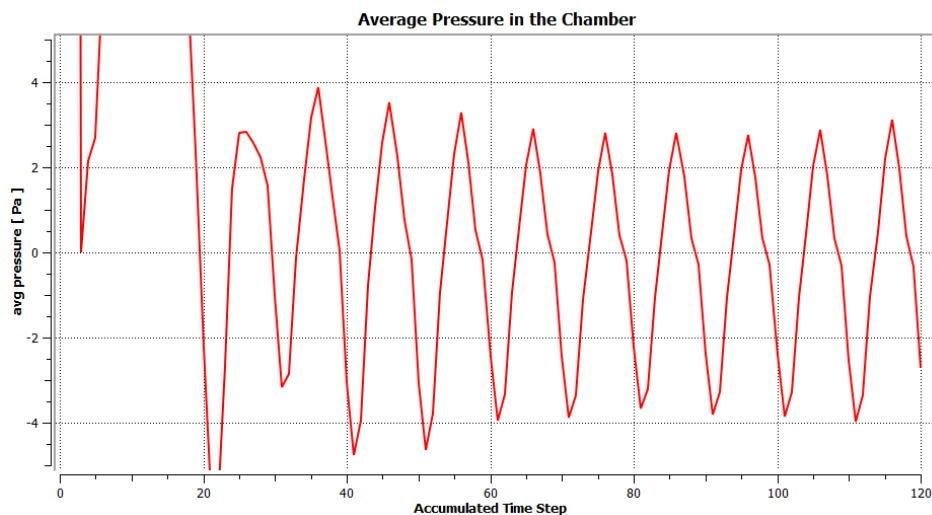


Figure 4.8: Air Pressure Graph of the Circular Bottom Profile U-OWC Chamber

4.2.5 Data Extraction from the Steady-State Time Steps

In order to gain a better observation on the performance of the U-OWC models, the simulation results which are corresponded to the time step range from 40 to 120 are averaged and plotted in graphs. This is because the air velocity variation and air pressure variation after the time step 40 are in stable state which will not cause large error to the averaged value of the simulation results.

4.2.6 Comparison of Simulation Results of the Four U-OWC Models

The averaged results of the simulated U-OWC models are shown in Figure 4.9. It is noticed that the average velocity produced by the U-OWCs with 1:1 slope and 1:5 slope bottom profiles are 26.33% and 16.65 %, respectively greater than that of the U-OWC with flat bottom profile. Additionally, average pressure generated by the U-OWCs with 1:1 slope and 1:5 slope bottom profiles are 1.64 times and 1.51 times correspondingly higher than that of the U-OWC with flat bottom profile. The results appear to draw a parallel to the findings from research conducted by Iino et al. (2016) which explained that the implementation of inclination angles of 40° to 45° on the OWC chamber bottom part can produce more plane area for water column and minimize the gravity effect. Besides, the slope bottom profile is able to reduce the water wave turbulence effect in the OWC chamber as well as extending the resonant period. In other words, the air discharge-velocity and air discharge-pressure will be enhanced.

On the other hand, Figure 4.9 also indicates that the flat bottom profile U-OWC produces the lowest average air velocity and average air pressure among the four models. This provides clear evidence for research results performed by Ashlin, Sundar and Sannasiraj (2016), for which the shape modification of the bottom profile can improve the performances of air column velocity and air column pressure for the U-OWC. The average velocity and average pressure produced by the circular bottom profile U-OWC are 27.38 % and 68.95 % greater than that of the conventional flat bottom profile U-OWC, respectively. The data also validates the research result conducted by Ashlin, Sundar and Sannasiraj (2016), specifically, the circular shape bottom profile is able to speed up the water wave entry motion, improves water surface oscillation and escalates the amplification factor of the water column.

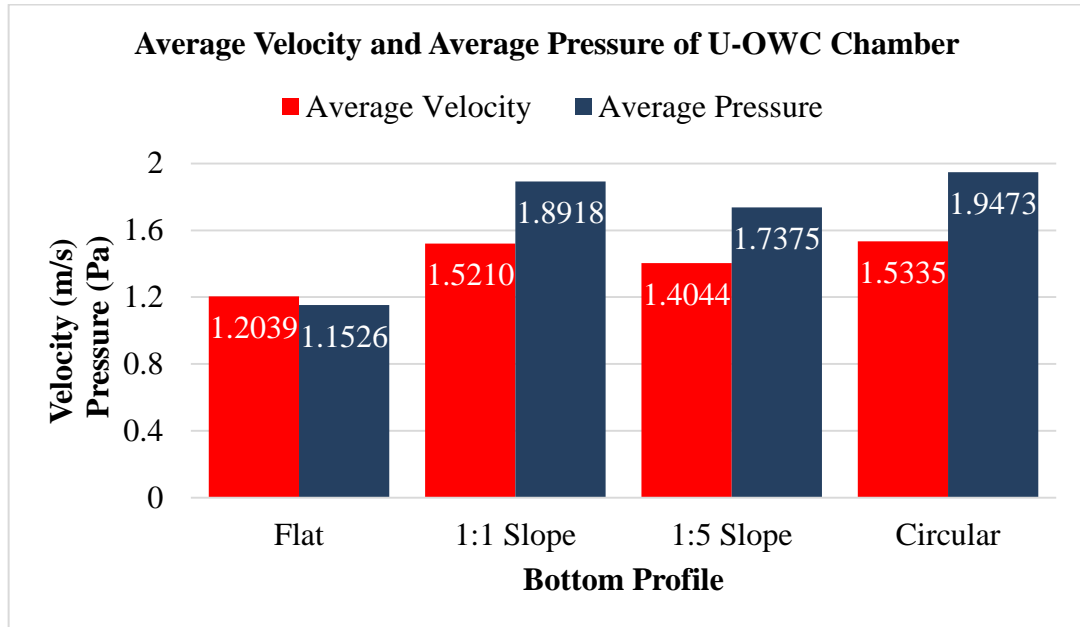


Figure 4.9: Results Comparison Chart for the Simulated U-OWC Models

4.2.7 Selection of the Optimum Bottom Profile of U-OWC

The power output for the simulated U-OWC models are computed from Equation 2.9 and the detail calculation steps are referred to Appendix F. According to the power outputs as shown in Table 4.1, the performance ranking for the bottom profile of the four U-OWC models can be expressed in increasing order of flat, 1:5 slope, 1:1 slope and circular.

Several inferences can be made from Table 4.1. First, the circular bottom profile U-OWC generates the greatest power output due to its dominant magnitudes in air velocity and air pressure. Next, it is observed that the power produced by the circular bottom profile U-OWC is about 2.15 times greater than that of the conventional flat bottom profile U-OWC and is only 3.78 % slightly higher than that of the second best bottom profile U-OWC, which is the 1:1 slope.

The circular bottom profile U-OWC is capable to yield average air velocity of 1.5335 m s^{-1} , average air pressure of 1.9473 Pa and power output of $2.1108 \times 10^{-3} \text{ W}$. Given these points, the circular bottom profile U-OWC is concluded to be the best design among all the four simulated U-OWC models.

Table 4.1: Summary of the Simulation Results

Bottom Profile	Average Velocity (m s^{-1})	Average Pressure (Pa)	Area of Orifice ($\times 10^{-4} \text{ m}^2$)	Power Output ($\times 10^{-3} \text{ W}$)
Flat	1.2039	1.1526	7.0686	0.9808
1:1 Slope	1.5210	1.8918	7.0686	2.0339
1:5 Slope	1.4044	1.7375	7.0686	1.7248
Circular	1.5335	1.9473	7.0686	2.1108

4.3 Experimental Results

The experimental results of air velocity and air pressure are shown in Figure 4.10 and Figure 4.11, respectively. According to Figure 4.10, the trend line shows a steep positive slope at the early stage and then followed by the stable state. The behaviour of trend line indicates that the experimental air velocity values increased significantly in the experimental time interval from 1 s to around 9 s which can be explained as the water wave's build-up stage. Whereas from the experimental time of 9 s onwards, it seems that the stable water waves have been built up and the fluctuations of the air velocity values are not apparently large and hence, this is termed as the stable state. Therefore, the air velocity values are averaged ranging from the experimental time interval of 9 s to 18 s in order to obtain a better analysis on the experimental results.

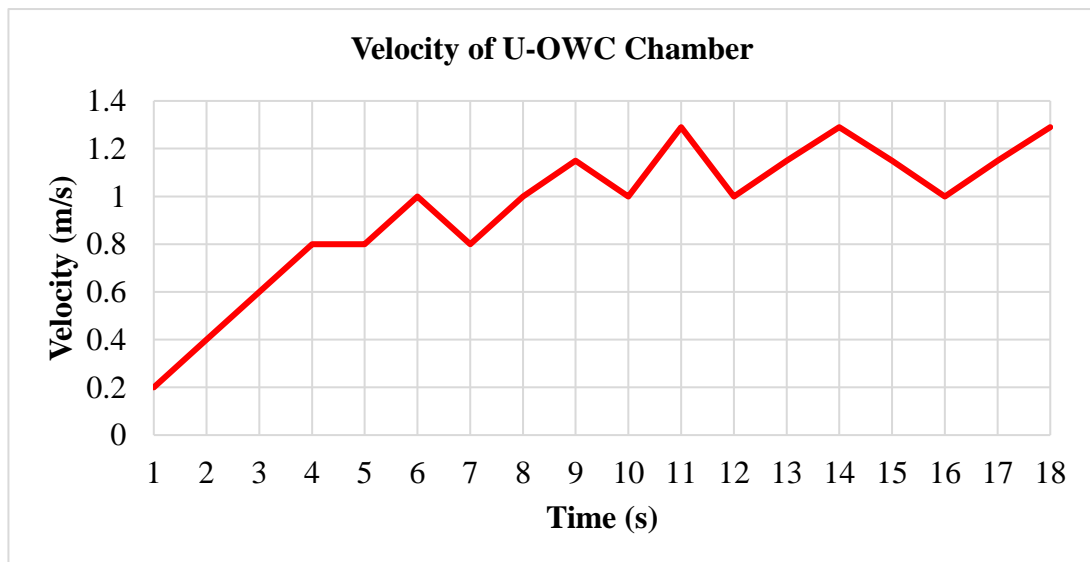


Figure 4.10: Air Velocity Graph of the U-OWC Prototype Chamber

In contrast to the trend line of air velocity, the trend line in Figure 4.11 shows that the air pressure values undergo large fluctuations along the entire experimental time interval of 18 s. The behaviour of trend line may contribute some degrees of error to the air pressure experimental results.

Besides, it is important to note that the experimental measurements of air pressure were taken for 18 s right after the measurements of air velocity because the measurements of the air velocity and air pressure could not be performed at the same time. The reason behind this is that the physical size of pressure sensor and anemometer are larger than the 3 cm orifice diameter and in order to avoid blockage of the air flow, both instruments have to take turns for positioning and to perform measurements at the top surface of orifice. Therefore, the air pressure values are averaged ranging from the experimental time interval of 1 s to 18 s in order to obtain a better examination on the experimental results.

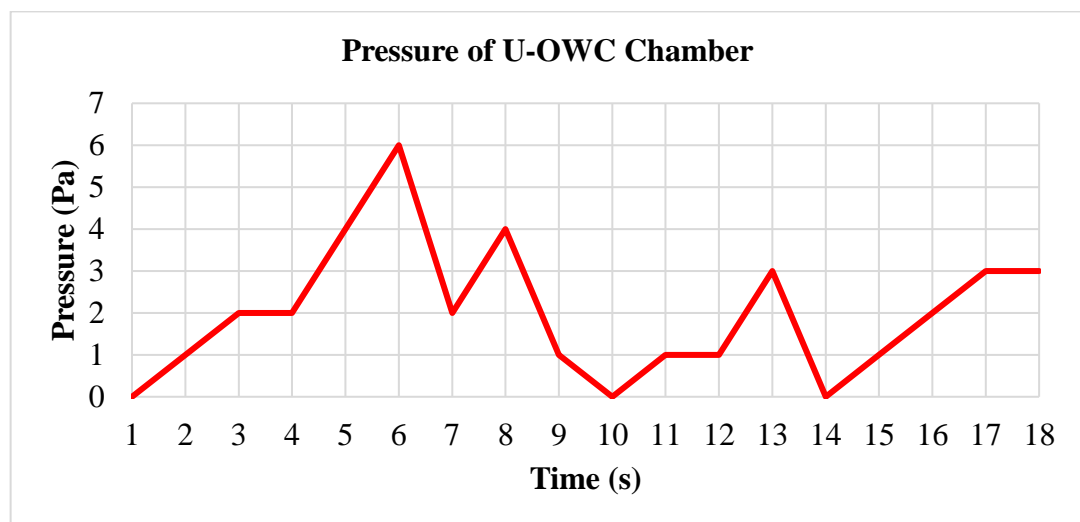


Figure 4.11: Air Pressure Graph of the U-OWC Prototype Chamber

4.3.1 Comparison of Average Velocity and Average Pressure between Optimum Simulated U-OWC and Experimental U-OWC

Figure 4.12 shows the result comparison chart for simulated optimum U-OWC and experimental U-OWC. In terms of average air velocity, the experimental value is about 33.7 % lower than the simulation value. The inconsistency may be due to the three experimental errors, namely (i) low stiffness of the paddles of the Arduino water wave generator, (ii) water waves whirl motions and (iii) single-directional air

velocity measurement. The detail explanations for these errors can be referred in Chapter 4.4.2.1, Chapter 4.4.2.3 and Chapter 4.4.2.4 respectively.

Contrary to the common expectation, which the experimental value will be lower than the simulated value, it is determined that the experimental average air pressure value is 8.75 % higher than the simulated average air pressure. A plausible explanation would be the occurrence of pressure sensor error. Notably, the measurements of the experimental pressure values were performed at the open air conditions and the windy air effect during the experiment was likely to affect the exactness and precision of the pressure sensor. The detail explanation of this error can be referred in Chapter 4.4.2.2.

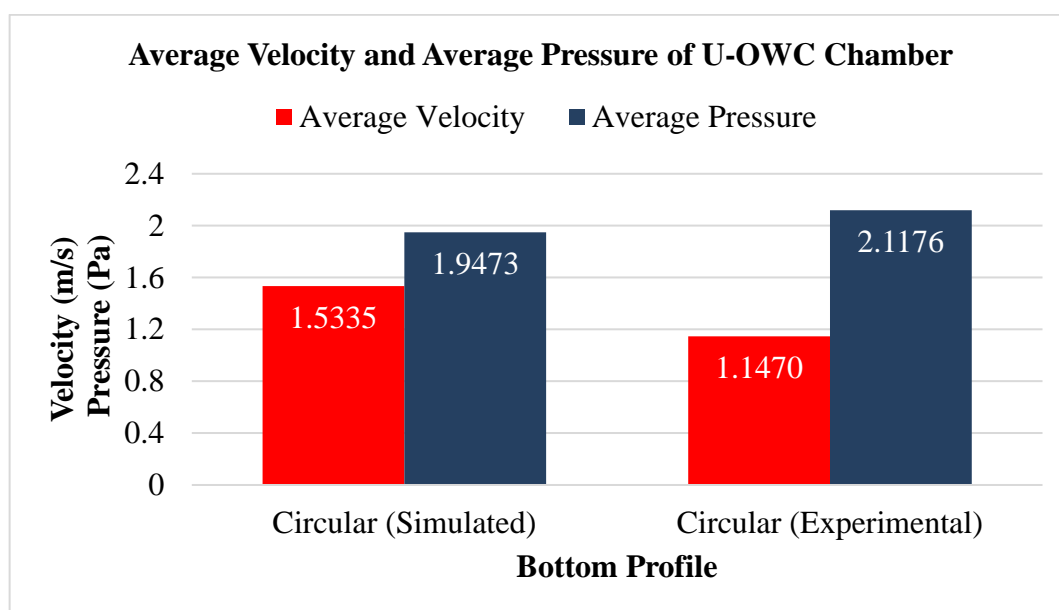


Figure 4.12: Results Comparison Chart of Simulation and Experimental

4.3.2 Comparison of Power Output between Optimum Simulated U-OWC and Experimental U-OWC

The power outputs for both cases are calculated from Equation 2.9 for which the power output is computed with the multiplications of orifice area, air velocity and air pressure. The detail steps are demonstrated in Appendix F. Figure 4.13 shows the performances comparison of the simulated and the experimental U-OWC with circular bottom profile. The comparison indicates that the experimental results are tolerably acceptable as the experimental results are 18.66 % deviated from the

simulation result. The deviation may due to the simulation error and experimental errors which will be explained in Chapter 4.4.

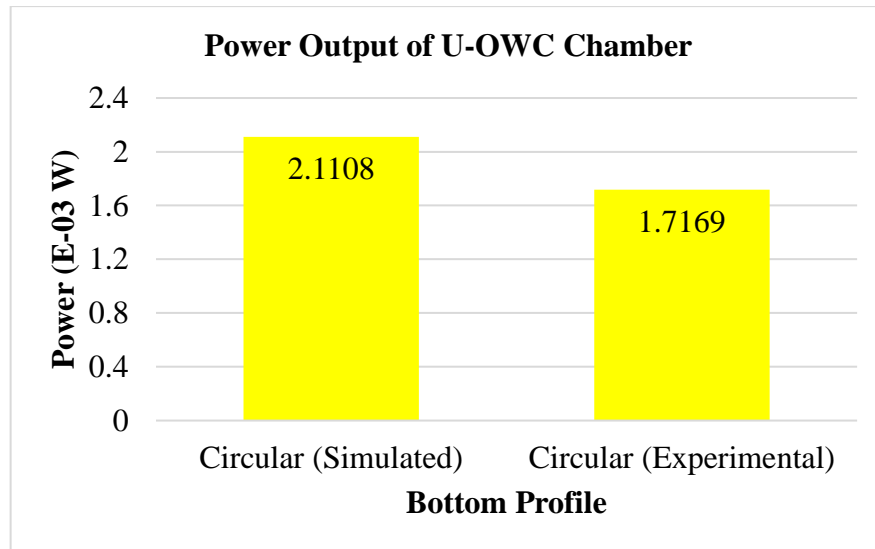


Figure 4.13: Power Output Comparison Chart of Simulation and Experimental

4.4 Causes of the Percentage Error

One simulation error and four experimental errors are labelled as the contributors for the percentage error between the simulation results and the experimental results.

4.4.1 Simulation Error

4.4.1.1 Time Step Error

Time step is crucial in simulation because it controls the accuracy of the solver or in other words, the resolution of the simulated results. The smaller the time step interval, the greater the resolution of the simulated data. Time step with smaller time interval requires longer time for solution generation (Albatayneh et al., 2015). Therefore, extension in solution generation time is required in order to obtain simulation results with higher resolution. Nonetheless, due to the limitations of the project computer specifications (detail explanation in Chapter 5.2), the total simulation time was set as 12 s along with larger time step interval of 0.1 s. This is because any settings of time step interval which are below 0.1 s will cause the fatal simulation error which is termed as the "Overflow in Linear Solver". As a result, the limitation of time step interval reduces the accuracy of the simulation results and rises the percentage error.

4.4.2 Experimental Errors

4.4.2.1 Low Stiffness of the Paddles of the Arduino Water Wave Generator

During the generation of water waves, the middle section of the paddles which faced the continuous back-and-forth motions were bent as illustrated in Figure 4.14. This issue happened because the paddles are made of 2 mm thick acrylic sheet and the high flexibility of these paddles could not withstand the heavy water pressure. The paddles were displaced to “S” shaped when there was a backward wave hitting the other side of the paddles. The generation of water wave became unstable during the bending of paddles which resulted the reduction of orifice air-discharge velocity.



Figure 4.14: Bending of the Paddles

4.4.2.2 Exposure of the Pressure Sensor to Ambient Conditions

For the ideal case, the pressure sensor should be installed inside the U-OWC chamber to minimize the sensor error caused by the atmospheric pressure. However, the measurements of the chamber air pressure were performed at the open air condition where the pressure sensor was placed on top of the chamber orifice. This is because the size of the breadboard-embedded pressure sensor was larger than orifice diameter and could not be installed inside the chamber. Consequently, the pressure measurements are almost similar to the atmospheric pressure and being affected by the windy air conditions. As a result, increment in percentage error is happened.

4.4.2.3 Water Waves Whirl Motions

The water tank is tolerably small in width which has caused the whirl motions during the water wave generation. This is because the narrow width of the water tank will

cause the tank walls to produce substantial amount of side water waves that weaken the amplitude of the generated waves. Subsequently, the values of air velocity and air pressure in the U-OWC chamber are diminished.

4.4.2.4 Single-directional Air Velocity Measurement

As a matter of fact, the simulated air velocity values include both the “inhalation” and “exhalation” of the U-OWC chamber and hence, the experimental air velocity should be measured with the bidirectional turbine equipment which only rotates in a single direction regardless of the air flow direction through the turbine as explained in the research conducted by Torre-Enciso et al. (2009).

Nevertheless, the digital anemometer which is used for the experimental measurements of air-discharge velocity from the prototype chamber was only able to measure the air velocities for the “exhalation” of the chamber because the turbine equipped in the anemometer is not a bidirectional turbine. Precisely, when the anemometer is held in parallel to the orifice surface as demonstrated in Figure 4.15, the chamber “exhalation” will cause clockwise turbine rotation and thus the air velocity is measured, while the chamber “inhalation” which will cause the anticlockwise turbine rotation will not happen because the air flow magnitude for “inhalation” is not sufficiently high enough to stop the previous clockwise turbine rotation and then to initiate the anticlockwise turbine direction.

As a result, the experimental air velocity values have excluded parts of the important air velocity data which is contributed by the chamber “inhalation” and this may be accounted for the happening of the fairly high percentage error of the experimental air velocity results.



Figure 4.15: Positioning of the Digital Anemometer during Experiment

CHAPTER 5

CONCLUSIONS AND RECOMMENDATIONS

5.1 Conclusions

This project has examined the effects of four different bottom profiles specifically, flat, 1:1 slope, 1:5 slope and circular on the performance of the U-OWC structure via ANSYS CFX simulation. From the simulation results, it was found that the 1:1 slope bottom profile and 1:5 slope bottom profile, had higher air velocity values than that of the conventional flat bottom profile U-OWC by 26.33 % and 16.65 % respectively. It was also found that the 1:1 slope bottom profile and 1:5 slope bottom profile, had higher air pressure values than that of the conventional flat bottom profile U-OWC by 1.64 times and 1.51 times correspondingly. A possible explanation for these results is that the inclined slope bottom profile increases the water column plane area, lowers the water column turbulence effect and enhances the air-discharge velocity and the air-discharge pressure.

Another finding from the simulation results is the power output yielded by the circular bottom profile U-OWC is 2.15 times better than the power output produced by the flat bottom profile U-OWC. This can be adequately explained by the circular shape bottom profile induces the acceleration of water wave entry motion, enhances water surface oscillation and increases the power output. Given the simulation results, the performance of the bottom profile can be ranked in increasing order as flat, 1:5 slope, 1:1 slope and circular.

Based on the optimised simulated parameters, the optimum circular U-OWC prototype was fabricated to verify the simulation result. From the experimental results, it was found that the experimental average air velocity is 33.7 % lower than that of the simulated average air velocity. The deviation may be due to the experimental errors of (i) low stiffness of the paddles of the Arduino water wave generator (ii) water waves whirl motions and (iii) single-directional air velocity measurement that reduce the experimental values of air-discharge velocity.

Whereas for the average air pressure, the experimental value appears to be 8.75 % greater than the simulated value. The slight percentage difference may be caused by the pressure sensor error which the air pressure measurements were

affected by the ambient conditions and windy air conditions. Moreover, the simulation time step error that reduces the resolution of the simulation results and the four experimental errors that cause uncertainties to the experimental results are accounted for the occurrence of 18.66 % percentage difference between the experimental power output and the simulated power output.

In conclusion, the findings of this project have proved that the circular bottom profile is the optimum bottom profile for the U-OWC structure that can generate the greatest air-discharge velocity, air-discharge pressure as well as the power output.

5.2 Problems Encountered in the Simulation Phase

5.2.1 Lengthy Time of Simulation Phase

According to Ozen Engineering Incorporation (2019), the minimum hardware requirements for the ANSYS CFD software are 4 processor cores and 16 gigabytes of random-access memory while the recommended specifications are 12 processor cores and 64 gigabytes of random-access memory. In this project, the computer achieved the minimum processor cores number of 4 but it has only 8 gigabytes of random-access memory which is only half of the minimum specification. Therefore, the data processing speed was slow and required extensive hours to complete the simulations.

5.2.2 Simulation Failure due to “Isolated Fluid Region” Error

The simulation fatal error of “Isolated Fluid Region” was caused by the wrong selection of the location for the opening boundary condition for the water domain. It is important to acknowledge that the particular location which is self-defined as the “interphase region” as shown in Figure 3.36 between the water domain and the air domain must not be selected by any boundary conditions. This step assists the ANSYS software to automatically recognize the existence of two separated domains and hence enabling the flow connection during the simulation.

5.2.3 Simulation Failure due to “Overflow in Linear Solver” Error

The simulation termination error of “Overflow in Linear Solver” was caused by the extreme small value of time step which the computer processor was not capable to

process such massive amount of the numerical data. In this case, time step of 0.1 s was used for the simulations and any values below 0.1 s will cause the error. In other words, appropriate time step value should be set to fit the computer specifications.

5.3 Problems Encountered in the Experimental Phase

5.3.1 Leaking Water Tank

This problem was caused by the low stiffness of the acrylic water tank wall. When the water tank was half filled by the water, the two long side tank walls were unable to withstand the water pressure, thus were bending outward. This has triggered the tank bottom adhesive layers to break and caused water leakage. Thereafter, the water was removed from the tank, let dry and silicon glue was reapplied onto the bottom side lines. Furthermore, a set of metal frames as illustrated in Figure 5.1 were fabricated and were installed around the “weak” spots of the tank wall to enhance the mechanical strength of the tank walls. As a result, the tank walls bending effect was minimized and did not caused water leakage.



Figure 5.1: Enhancement Frames for Tank Walls

5.3.2 Mechanical Failure of the Arm-linkages of the Servo Motors

The first version of servo motors arm-linkages were built by metal strings with diameter of 1 mm as shown in Figure 5.2, however the 1 mm metal strings were not able to produce the back-and-forth paddles motion due to the bending of the metal strings which was caused by the high water pressure. Subsequently, the 1 mm metal

strings were replaced by 2 mm metal strings to increase the mechanical strength of the arm-linkages.



Figure 5.2: Servo Motor Arm-linkage

5.3.3 Synchronization of the Paddles Motions of the Arduino Water Wave Generator

The deviation in motions for the two separated paddles during the experiment has caused the unsteady water wave generation and water whirl motions. Hence, the process of synchronization of the paddles was performed and it required two important steps. First, the different in lengths of two metal strings that connects the paddle and the servo motor arm must be minimized to ensure uniform angular displacements. Second, the initial angular displacement of the servo motors arms must be programmed by Arduino to set as zero degree to ensure both servo motors arms operate at the same speed and same angular displacement during the experiment.

5.4 Limitations of the Project

The project were restricted by three notable limitations as below:

- i. The low specifications of the project computer with 8 gigabytes of random-access memory and 4 processor cores have confined the simulation setup to smaller meshing size and larger time step that affected the accuracy of the simulation results.
- ii. The tolerably small width of water tank has caused the water wave whirl motions during the experiment and increased the percentage error.
- iii. The low stiffness of acrylic water tank was not capable to withstand high water pressure and caused outward bending of the water tank walls.

5.5 Recommendations for the Future Project

Four potential steps to improve the future project are computed as:

- i. Computer with random-access memory of 64 gigabytes and 12 processor cores should be implemented for the ANSYS simulation to improve the meshing capability and to increase the processing speed of the simulation.
- ii. The width of the water tank should be increased to 3 times greater than the current size that could certainly prevent the occurrence of water wave whirl motions
- iii. The water tank should be made of glass instead of the flexible acrylic and the thickness of water tank is recommended to increase by 5 mm which results the 10 mm wall thickness that could withstand the high water wall pressure.

REFERENCES

- Albatayneh, A., Alterman, D., Page, A. and Moghtaderi, B., 2015. The significance of time step size in simulating the thermal performance of buildings. *Advances in Research*, 5(6), pp.1–12.
- Ashlin, S.J., Sundar, V. and Sannasiraj, S.A., 2016. Effects of bottom profile of an oscillating water column device on its hydrodynamic characteristics. *Renewable Energy*, 96, pp.341–353.
- Boccotti, P., 2007. Comparison between a U-OWC and a conventional OWC. *Ocean Engineering*, 34(5–6), pp.799–805.
- Bouali, B. and Larbi, S., 2013. Contribution to the geometry optimization of an oscillating water column wave energy converter. *Energy Procedia*, 36, pp.565–573.
- Central Intelligence Agency, 2018. *The world factbook*. [online] Available at: <<https://www.cia.gov/library/publications/the-world-factbook/fields/2060.html>> [Accessed 23 Jun. 2018].
- Falcão, A.F.O. and Henriques, J.C.C., 2014. Model-prototype similarity of oscillating-water column wave energy converters. *International Journal of Marine Energy*, 6, pp.18–34.
- Falcão, A.F.O. and Henriques, J.C.C., 2016. Oscillating-water-column wave energy converters and air turbines: A review. *Renewable Energy*, 85, pp.1391–1424.
- Fried, L. and Townsend, K., 2019. *Arduino test Adafruit BME280*. [online] Available at: <<https://learn.adafruit.com/adafruit-bme280-humidity-barometric-pressure-temperature-sensor-breakout/arduino-test>> [Accessed 31 Mar. 2019].
- Hsieh, M., Lin, I.-H., Dorrell, D.G., Hsieh, M.-J. and Lin, C.-C., 2012. Development of a wave energy converter using a two chamber oscillating water column. 3(3), pp.482–497.
- Iino, M., Miyazaki, T., Segawa, H. and Iida, M., 2016. Effect of inclination on oscillation characteristics of an oscillating water column wave energy converter. *Ocean Engineering*, 116, pp.226–235.
- Malara, G., Gomes, R.P.F., Arena, F., Henriques, J.C.C., Gato, L.M.C. and Falcão, A.F.O., 2017. The influence of three-dimensional effects on the performance of U-type oscillating water column wave energy harvesters. *Renewable Energy*, 111, pp.506–522.
- Mora, A., Bautista, E. and Méndez, F., 2017. Influence of a tapered and slender wave collector on the increment of the efficiency of an oscillating water column wave-energy converter. *Ocean Engineering*, 129(October 2016), pp.20–36.

Muda, N. and Tey, J.P., 2012. On prediction of depreciation time of fossil fuel in Malaysia. *Journal of Mathematics and Statistics*, [online] 8(1), pp.136–143. Available at: <<http://thescipub.com/pdf/10.3844/jmssp.2012.136.143>> [Accessed 22 Jun. 2018].

Office of Energy Efficiency & Renewable Energy, 2018. *Marine and hydrokinetic technology glossary*. [online] U.S. Department Of Energy. Available at: <<https://www.energy.gov/eere/water/marine-and-hydrokinetic-technology-glossary>> [Accessed 21 Jul. 2018].

Ozen Engineering Incorporation, 2019. *ANSYS system hardware requirements*. [online] Available at: <<https://www.ozeninc.com/ansys-system-hardware-requirements/>> [Accessed 28 Mar. 2019].

Samrat, N.H.S., Ahmad, N.B.A., Choudhury, I. and Taha, Z., 2014. Prospect of wave energy in Malaysia. *Proceedings of the 2014 IEEE 8th International Power Engineering and Optimization Conference, PEOCO 2014*, (March), pp.127–132.

SAS IP Incorporated, 2018a. *32.1.2. Displaying contours and profiles*. [online] Available at: <https://www.sharcnet.ca/Software/Ansys/17.0/en-us/help/flu_ug/flu_ug_sec_graphics_contours.html> [Accessed 20 Aug. 2018].

SAS IP Incorporated, 2018b. *5.1. Mesh topologies*. [online] Available at: <https://www.sharcnet.ca/Software/Ansys/17.0/en-us/help/flu_ug/flu_ug_GridTypes.html> [Accessed 20 Aug. 2018].

Shalby, M., Walker, P. and Dorrell, D.G., 2017. Modelling of the multi-chamber oscillating water column in regular waves at model scale. *Energy Procedia*, [online] 136, pp.316–322. Available at: <www.sciencedirect.com> [Accessed 11 Jun. 2018].

Sharma, A., 2017. *Introduction to computational fluid dynamics: development, application and analysis*.

Sheng, W., Alcorn, R. and Lewis, A., 2013. On thermodynamics in the primary power conversion of oscillating water column wave energy converters. *Journal of Renewable and Sustainable Energy*, 5(2).

Simonetti, I., Cappiotti, L., Elsafti, H. and Oumeraci, H., 2017. Evaluation of air compressibility effects on the performance of fixed OWC wave energy converters using CFD modelling. *Renewable Energy*, [online] 119, pp.741–753. Available at: <<http://linkinghub.elsevier.com/retrieve/pii/S0960148117312235>>.

The Queen’s University of Belfast, 2002. Islay LIMPET wave power plant. [online] (April), pp.1–62. Available at: <https://cordis.europa.eu/docs/publications/6662/66628981-6_en.pdf>.

Torre-Enciso, Y., Ortubia, I., López de Aguilera, L.I. and Marqués, J., 2009. Mutriku wave power plant: from the thinking out to the reality. *8th European Wave and Tidal Energy Conference (EWTEC 2009)*, [online] pp.319–328. Available at: <http://tethys.pnnl.gov/sites/default/files/publications/Torre-Enciso_et_al_2009.pdf>.

United Nations, 2015. *World population prospects: The 2015 revision, key findings and advance tables*. [online] New York. Available at: <https://esa.un.org/unpd/wpp/Publications/Files/Key_Findings_WPP_2015.pdf> [Accessed 21 Jun. 2018].

Vyzikas, T., Deshoulières, S., Barton, M., Giroux, O., Greaves, D. and Simmonds, D., 2017. Experimental investigation of different geometries of fixed oscillating water column devices. *Renewable Energy*, 104, pp.248–258.

Zaoui, L., Bouali, B., Larbi, S. and Benchatti, A., 2014. Performance analysis of a 3D axisymmetric oscillating water column. *Energy Procedia*, 50, pp.246–254.

APPENDICES

APPENDIX A: Excel Calculation of Average Velocity of Simulation Results

Flat		1to1		1to5		Curved	
Series 1 at avg vel							
[Data]		[Data]		[Data]		[Data]	
Accumulated Time Step	avg vel [m s ⁻¹]	Accumulated Time Step	avg vel [m s ⁻¹]	Accumulated Time Step	avg vel [m s ⁻¹]	Accumulated Time Step	avg vel [m s ⁻¹]
0		0		0		0	
1	1.04991841	1	17.3309498	1	1.37598157	1	11.4510727
2	1.26939988	2	7.96581268	2	1.34782207	2	6.96851873
3	1.91287732	3	8.08427715	3	1.86210203	3	8.98174953
4	2.48299408	4	2.10400844	4	2.37128568	4	6.79799938
5	3.01993132	5	1.37444758	5	2.94211984	5	5.39834785
6	3.46993494	6	1.28874731	6	3.46268559	6	4.26188755
7	3.70547819	7	1.74674189	7	3.76731086	7	3.37632513
8	3.67903686	8	2.23216605	8	3.84696293	8	2.92006254
9	3.40256095	9	2.58091617	9	3.66819334	9	2.74643874
10	2.86637235	10	3.00383544	10	3.07524729	10	2.61669666
11	2.17044425	11	3.03534102	11	2.20563316	11	2.30298352
12	1.26408517	12	2.47031474	12	1.1192683	12	1.60480332
13	0.190935686	13	1.51900268	13	0.464880228	13	0.6009534
14	1.14352536	14	0.69532901	14	1.52239108	14	0.525929093
15	1.54273951	15	0.377548307	15	1.91393054	15	0.709230781
16	1.1644603	16	0.680371881	16	1.57275832	16	0.27849552
17	0.525617182	17	1.36155558	17	0.830615342	17	0.573578179
18	0.092274986	18	2.24955606	18	0.2222839	18	1.54156232
19	0.951269388	19	3.22013712	19	1.29744732	19	2.6780057
20	1.75109506	20	4.06319094	20	2.14438272	20	3.65126657
21	2.16281557	21	4.49933767	21	2.53588724	21	4.16800356
22	2.17121029	22	4.27537489	22	2.23642206	22	4.07765579
23	1.91661596	23	3.29638195	23	1.81803548	23	3.24092722
24	1.29172194	24	1.8089745	24	1.18119049	24	1.77770472
25	0.745391071	25	0.446963578	25	0.550587535	25	0.470940858
26	0.574419439	26	0.32991761	26	0.255742669	26	0.530184925
27	0.789362073	27	0.276935041	27	0.35246712	27	0.428104132
28	1.12983143	28	0.413383275	28	0.782276571	28	0.262207419
29	1.44423711	29	1.23782241	29	1.52212989	29	1.25671554
30	1.74299717	30	2.09250522	30	2.07038331	30	2.35256267
31	1.72643006	31	2.51714444	31	2.21830988	31	2.95271802
32	1.44716942	32	2.30351424	32	1.83745706	32	2.77713728
33	0.541873515	33	1.12262368	33	0.733255446	33	1.71782625
34	0.746685624	34	0.72385031	34	0.530180871	34	0.298774481
35	1.27005219	35	1.54038894	35	1.35923874	35	1.34773684
36	1.18573976	36	1.46280515	36	1.19892323	36	1.64028382
37	0.566327274	37	0.663993061	37	0.783576071	37	1.13452709
38	0.478732765	38	0.740309358	38	0.329061061	38	0.140761256
39	1.54427624	39	2.0295043	39	1.67656767	39	1.51791048
40	2.18824983	40	2.84335232	40	2.68179965	40	2.65326238
41	2.19603968	41	3.10750175	41	2.88064766	41	3.08922601
42	1.83082247	42	2.78613663	42	2.4449935	42	2.81938624
43	0.898317814	43	1.30243623	43	1.20234215	43	1.64488637
44	0.390002608	44	0.602399945	44	0.431976795	44	0.454854965
45	1.02121389	45	1.53390622	45	1.20186925	45	1.48057294
46	1.1341908	46	1.63857436	46	1.21098781	46	1.8074007
47	0.67211771	47	0.981363952	47	0.811132193	47	1.32813549
48	0.357996643	48	0.304779202	48	0.227828309	48	0.340551049
49	1.52224529	49	1.75250828	49	1.65884435	49	1.31440985
50	2.25782847	50	2.7952435	50	2.73434305	50	2.51136875

APPENDIX B: Excel Calculation of Average Pressure of Simulation Results

Flat		1to1		1to5		Curved	
Series 1 at avg pressure							
[Data]		[Data]		[Data]		[Data]	
Accumula avg pressure [Pa]		Accumula avg pressure [Pa]		Accumula avg pressure [Pa]		Accumula avg pressure [Pa]	
0	10.8392315	0	0	0	10.8392315	0	10.8392315
1	2.74235535	1	1173.37109	1	2.44851565	1	1480.46448
2	2.44690418	2	-1850.65222	2	1.6189754	2	78.9972458
3	1.72083187	3	-576.053467	3	1.89161348	3	-0.005316756
4	-0.324716985	4	-18.288208	4	0.617801011	4	2.13306546
5	-2.66132474	5	26.0234489	5	-1.51101267	5	2.69479132
6	-4.74052811	6	49.9010506	6	-3.95164061	6	6.22034836
7	-6.2078867	7	60.6690826	7	-6.18690348	7	7.63752079
8	-6.71539259	8	56.3099174	8	-7.41711998	8	7.82834196
9	-6.04203701	9	42.9477539	9	-6.89252901	9	6.92284584
10	-4.26959181	10	39.180706	10	-4.49997377	10	6.24188519
11	-2.25177002	11	33.785759	11	-1.86451411	11	6.56909132
12	-0.365574062	12	29.7999916	12	0.143689334	12	7.58625174
13	0.578733146	13	28.5843658	13	1.04765344	13	8.18613243
14	1.65597463	14	28.5068493	14	3.011621	14	8.4162178
15	2.37735486	15	26.3141079	15	4.1570878	15	8.56180382
16	1.4395225	16	23.9606361	16	2.95660257	16	7.89766884
17	0.615037024	17	21.6047325	17	1.25067592	17	7.40619707
18	0.440210164	18	17.1668682	18	0.586168885	18	5.89088583
19	0.010294234	19	9.83519745	19	-0.332783639	19	2.37001085
20	-1.36273408	20	2.61960554	20	-2.20423055	20	-2.20656061
21	-2.43611193	21	-2.50564647	21	-3.42012787	21	-5.62112951
22	-2.54273319	22	-3.99047017	22	-2.63071847	22	-5.94170856
23	-1.98319328	23	-1.66471171	23	-1.71666873	23	-2.69341063
24	-0.73402369	24	1.81678593	24	-0.53656143	24	1.49122548
25	-0.067583539	25	3.2236197	25	0.125900373	25	2.80857992
26	0.028361369	26	3.2405467	26	0.238295138	26	2.84102082
27	-0.166632235	27	2.90665174	27	0.175301194	27	2.56309032
28	-0.55949688	28	2.55021071	28	-0.131027445	28	2.23299456
29	-1.06146371	29	1.56935382	29	-1.18115222	29	1.5611558
30	-1.67077708	30	-0.553404152	30	-2.39539814	30	-1.00593925
31	-1.63878715	31	-2.1018703	31	-2.80190539	31	-1.6354012
32	-1.12136745	32	-1.74407399	32	-1.8565619	32	-2.8459847
33	0.028085342	33	0.633118689	33	-0.077041216	33	-0.153142273
34	0.773504078	34	1.92868447	34	0.599173307	34	1.70688677
35	1.46802342	35	3.53429389	35	1.90750265	35	3.16713905
36	1.30211747	36	3.36496925	36	1.52300992	36	3.87338424
37	0.340438336	37	1.69074392	37	0.718007147	37	6.27347771
38	-0.063964106	38	0.875200748	38	0.030295711	38	1.3173058
39	-1.26047587	39	-1.2759949	39	-1.4689486	39	0.037440963
40	-2.74592233	40	-3.91976023	40	-4.18272781	40	-3.04463673
41	-2.78116679	41	-5.06188393	41	-4.86100721	41	-4.76497555
42	-1.93925154	42	-4.02979088	42	-3.48719931	42	-3.96079111
43	-0.352100074	43	-0.349084705	43	-0.687333822	43	-0.786091864
44	0.376611233	44	1.04844391	44	0.416081309	44	1.04849422
45	1.02389693	45	2.71526098	45	1.61942589	45	2.573531
46	1.21959639	46	3.07740831	46	1.54442096	46	3.51761866
47	0.467314869	47	1.49574518	47	0.738222778	47	2.25601172
48	-0.028290208	48	0.473249257	48	0.059037477	48	0.759806395
49	-1.22423434	49	-1.07092094	49	-1.4201262	49	-0.168055192
50	-2.94098639	50	-4.10715246	50	-4.36342478	50	-3.07173228
51	-2.97772789	51	-5.0100131	51	-5.16422558	51	-4.64090395
52	-1.94859552	52	-2.91575336	52	-3.64899564	52	-3.78803635
53	-0.25611622	53	0.051323112	53	-0.792346776	53	-0.949706137
54	0.45515424	54	1.26101303	54	0.405986637	54	0.686360121
55	1.19623899	55	3.01013112	55	1.8536371	55	2.31484151
56	1.38960433	56	2.90952158	56	1.78389335	56	3.27975774
57	0.551870644	57	1.17693591	57	0.928043723	57	2.11565018
58	0.005855105	58	0.308487892	58	0.051407531	58	0.521627784
59	-0.915116131	59	-1.47058702	59	-1.07985449	59	-0.158960596
60	-2.54661751	60	-3.65235662	60	-3.80488491	60	-2.46252871
61	-2.72234726	61	-4.21077585	61	-4.78947353	61	-3.95949841
62	-1.84505701	62	-3.19083977	62	-3.49616027	62	-3.33022475
63	-0.273860395	63	-0.313211083	63	-0.880826354	63	-0.955891848
64	0.401566923	64	0.883812606	64	0.273170143	64	0.565257251
65	0.992375851	65	2.46570563	65	1.40351272	65	2.03574395
66	1.08099639	66	2.73243356	66	1.25943732	66	2.90419984
67	0.352210939	67	1.18204844	67	0.653879702	67	1.84548187
68	-0.02741087	68	0.297951758	68	-0.00057279	68	0.4198125
69	-0.107406664	69	-1.13025784	69	-1.28020525	69	-0.232752547
70	-2.6118958	70	-3.2414465	70	-3.82849479	70	-2.43503928
71	-2.69879556	71	-3.84502602	71	-4.69560337	71	-3.89025545
72	-1.84273875	72	-2.94814992	72	-3.46023202	72	-3.35738492
73	-0.368577868	73	-0.368347347	73	-1.05397701	73	-1.10926974
74	0.366501749	74	0.713941038	74	0.205020785	74	0.471189708
75	0.979078472	75	2.11398244	75	1.24628055	75	1.90728593
76	1.12817717	76	2.36089706	76	1.21917498	76	2.80626011
77	0.40771438	77	1.01961517	77	0.646718383	77	1.83328092
78	-0.024773704	78	0.24579075	78	-0.00743932	78	0.394216776

79	-0.900922656	0.900922656		79	-1.15044582	1.15044582		79	-1.07250011	1.07250011		79	-0.190682039	0.190682039
80	-2.29583931	2.29583931		80	-3.25566435	3.25566435		80	-3.4219327	3.4219327		80	-2.21906519	2.21906519
81	-2.44685268	2.44685268		81	-3.93355727	3.93355727		81	-4.33247328	4.33247328		81	-3.66594338	3.66594338
82	-1.69156432	1.69156432		82	-3.13206649	3.13206649		82	-3.29859805	3.29859805		82	-3.20757699	3.20757699
83	-0.326488405	0.326488405		83	-0.559179604	0.559179604		83	-1.03810191	1.03810191		83	-1.06505191	1.06505191
84	0.394587696	0.394587696		84	0.558805466	0.558805466		84	0.154574528	0.154574528		84	0.432769567	0.432769567
85	0.983324647	0.983324647		85	1.82765007	1.82765007		85	1.07055068	1.07055068		85	1.92408061	1.92408061
86	1.04772294	1.04772294		86	2.1434176	2.1434176		86	0.961747944	0.961747944		86	2.81494737	2.81494737
87	0.341730595	0.341730595		87	0.914253294	0.914253294		87	0.505895853	0.505895853		87	1.77903509	1.77903509
88	-0.041349046	0.041349046		88	0.193458319	0.193458319		88	-0.037589852	0.037589852		88	0.335823655	0.335823655
89	-1.00389218	1.00389218		89	-1.11056936	1.11056936		89	-1.11125004	1.11125004		89	-0.274951309	0.274951309
90	-2.4030273	2.4030273		90	-3.12497544	3.12497544		90	-3.45796561	3.45796561		90	-2.3764894	2.3764894
91	-2.4995513	2.4995513		91	-3.82481027	3.82481027		91	-4.32505417	4.32505417		91	-3.79850245	3.79850245
92	-1.72419775	1.72419775		92	-3.07383251	3.07383251		92	-3.27371955	3.27371955		92	-3.27976537	3.27976537
93	-0.349687666	0.349687666		93	-0.615633786	0.615633786		93	-0.997901917	0.997901917		93	-1.08261216	1.08261216
94	0.383117706	0.383117706		94	0.478749603	0.478749603		94	0.153883576	0.153883576		94	0.408107191	0.408107191
95	1.00750637	1.00750637		95	1.68453658	1.68453658		95	0.913601696	0.913601696		95	1.92199051	1.92199051
96	1.09524322	1.09524322		96	2.04020095	2.04020095		96	1.03985012	1.03985012		96	2.76508808	2.76508808
97	0.383148104	0.383148104		97	0.882264256	0.882264256		97	0.542446375	0.542446375		97	1.7680552	1.7680552
98	-0.040831417	0.040831417		98	0.187966496	0.187966496		98	-0.023560869	0.023560869		98	0.325578034	0.325578034
99	-0.948158264	0.948158264		99	-1.04683268	1.04683268		99	-1.0240736	1.0240736		99	-0.283677399	0.283677399
100	-2.34452605	2.34452605		100	-3.03432345	3.03432345		100	-3.3039186	3.3039186		100	-2.41120648	2.41120648
101	-2.45723319	2.45723319		101	-3.74759531	3.74759531		101	-4.23196268	4.23196268		101	-3.84635925	3.84635925
102	-1.69298828	1.69298828		102	-3.06321621	3.06321621		102	-3.25175595	3.25175595		102	-3.28017378	3.28017378
103	-0.32013616	0.32013616		103	-0.721566856	0.721566856		103	-1.02656305	1.02656305		103	-1.06184709	1.06184709
104	0.421608955	0.421608955		104	0.419454813	0.419454813		104	0.094330542	0.094330542		104	0.432415336	0.432415336
105	1.07821417	1.07821417		105	1.54379261	1.54379261		105	1.03279078	1.03279078		105	2.03490782	2.03490782
106	1.13929105	1.13929105		106	1.88796747	1.88796747		106	1.00932825	1.00932825		106	2.87505984	2.87505984
107	0.39374423	0.39374423		107	0.802620709	0.802620709		107	0.573789835	0.573789835		107	1.80318534	1.80318534
108	-0.042329673	0.042329673		108	0.14605394	0.14605394		108	-0.030971322	0.030971322		108	0.323499091	0.323499091
109	-0.99230361	0.99230361		109	-1.02363443	1.02363443		109	-1.01766062	1.01766062		109	-0.307093352	0.307093352
110	-2.43141603	2.43141603		110	-2.93239832	2.93239832		110	-3.30128527	3.30128527		110	-2.5350523	2.5350523
111	-2.52617168	2.52617168		111	-3.61729312	3.61729312		111	-4.29200411	4.29200411		111	-3.98220277	3.98220277
112	-1.72619176	1.72619176		112	-2.98957491	2.98957491		112	-3.32580733	3.32580733		112	-3.34703898	3.34703898
113	-0.321656823	0.321656823		113	-0.710632801	0.710632801		113	-1.10639369	1.10639369		113	-1.04000688	1.04000688
114	0.441898257	0.441898257		114	0.397869617	0.397869617		114	0.134437889	0.134437889		114	0.483929753	0.483929753
115	1.12031698	1.12031698		115	1.43872833	1.43872833		115	1.03949797	1.03949797		115	2.20221519	2.20221519
116	1.17694855	1.17694855		116	1.81330884	1.81330884		116	1.02536464	1.02536464		116	3.13013458	3.13013458
117	0.405238926	0.405238926		117	0.78087461	0.78087461		117	0.519575238	0.519575238		117	1.97551572	1.97551572
118	-0.047047455	0.047047455		118	0.144059911	0.144059911		118	-0.025402214	0.025402214		118	0.37390849	0.37390849
119	-0.984231293	0.984231293		119	-1.01707506	1.01707506		119	-1.00521564	1.00521564		119	-0.343537629	0.343537629
120	-2.44384742	2.44384742		120	-2.88465619	2.88465619		120	-3.34057903	3.34057903		120	-2.69646907	2.69646907
		1.15255				1.891785482				1.737510736				1.947289818

APPENDIX C: Excel Calculation of Average Velocity of Experimental Results

Time (s)	Velocity Measured (m/s)
1	0.2
2	0.4
3	0.6
4	0.8
5	0.8
6	1
7	0.8
8	1
9	1.15
10	1
11	1.29
12	1
13	1.15
14	1.29
15	1.15
16	1
17	1.15
18	1.29
Average Velocity (m/s)	1.147

APPENDIX D: Screenshots of Pressure Data of Experimental Results

Temperature = 30.32 *C Pressure = 1002.93 hPa Approx. Altitude = 86.30 m Humidity = 69.75 %	Temperature = 30.33 *C Pressure = 1002.92 hPa Approx. Altitude = 86.32 m Humidity = 69.72 %	Temperature = 30.32 *C Pressure = 1002.90 hPa Approx. Altitude = 86.54 m Humidity = 69.71 %
Temperature = 30.33 *C Pressure = 1002.92 hPa Approx. Altitude = 86.35 m Humidity = 69.75 %	Temperature = 30.33 *C Pressure = 1002.88 hPa Approx. Altitude = 86.71 m Humidity = 69.71 %	Temperature = 30.32 *C Pressure = 1002.90 hPa Approx. Altitude = 86.47 m Humidity = 69.72 %
Temperature = 30.33 *C Pressure = 1002.90 hPa Approx. Altitude = 86.53 m Humidity = 69.74 %	Temperature = 30.32 *C Pressure = 1002.87 hPa Approx. Altitude = 86.75 m Humidity = 69.70 %	Temperature = 30.32 *C Pressure = 1002.89 hPa Approx. Altitude = 86.63 m Humidity = 69.71 %
Temperature = 30.33 *C Pressure = 1002.88 hPa Approx. Altitude = 86.68 m Humidity = 69.73 %	Temperature = 30.32 *C Pressure = 1002.87 hPa Approx. Altitude = 86.75 m Humidity = 69.69 %	Temperature = 30.32 *C Pressure = 1002.87 hPa Approx. Altitude = 86.78 m Humidity = 69.72 %
Temperature = 30.33 *C Pressure = 1002.84 hPa Approx. Altitude = 87.00 m Humidity = 69.73 %	Temperature = 30.32 *C Pressure = 1002.88 hPa Approx. Altitude = 86.66 m Humidity = 69.69 %	Temperature = 30.32 *C Pressure = 1002.90 hPa Approx. Altitude = 86.51 m Humidity = 69.69 %
Temperature = 30.33 *C Pressure = 1002.90 hPa Approx. Altitude = 86.56 m Humidity = 69.73 %	Temperature = 30.32 *C Pressure = 1002.87 hPa Approx. Altitude = 86.42 m Humidity = 69.71 %	Temperature = 30.32 *C Pressure = 1002.93 hPa Approx. Altitude = 86.30 m Humidity = 69.69 %

APPENDIX E: Excel Calculation of Average Pressure of Experimental Results

Pressure Measured (Pa)	Pressure Deviation (Pa)
100293	-
100292	1
100290	2
100288	2
100284	4
100290	6
100292	2
100288	4
100287	1
100287	0
100288	1
100287	1
100290	3
100290	0
100289	1
100287	2
100290	3
100293	3
Average Pressure (Pa)	2.117647

APPENDIX F: Calculations of Orifice Area, Power Output and Percentage Error

Orifice Area

$$A = \pi (r^2)$$

$$A = \pi (0.015^2)$$

$$A = 7.0686 \times 10^{-4} \text{ m}^2$$

Power Output

$$P_{PTO} = pQ_p$$

$$P_{PTO} = pAv$$

Sample calculation for experimental power output:

$$P_{PTO} = (2.1176)(7.0686 \times 10^{-4})(1.147)$$

$$P_{PTO} = 1.7169 \times 10^{-3} \text{ W}$$

Percentage Error

$$\% \text{ error} = \frac{\text{Simulated Value} - \text{Experimental Value}}{\text{Simulated Value}} \times 100$$

Sample calculation for percentage error of power outputs between simulation and experimental:

$$\% \text{ error} = \frac{2.1108 \times 10^{-3} - 1.7169 \times 10^{-4}}{2.1108 \times 10^{-4}} \times 100$$

$$\% \text{ error} = 18.6612 \%$$

APPENDIX G: Coding of the Servo Motor

```

sketch_mar21a
#include <Servo.h>

Servo myservoleft; // create servo object to control a servo motor arm
Servo myservoright;

int delaytime = 0;
int input = 0;

int previous = 0;
int current = 0;
int Status = 0;

void setup() {
  pinMode(A1, INPUT);

  Serial.begin(9600);
  myservoleft.attach(8); //connects the signal wire of left servo motor to pin 8
  myservoright.attach(9); //connects the signal wire of right servo motor to pin 9
  delay(100); //respond time
  myservoleft.write(0); //set to 0 degree
  myservoright.write(0); //set to 0 degree
  delay(3000);
}

void loop() {
  // put the main code here, to run repeatedly
  input = analogRead(A1);
  delaytime = 690; //to define paddles' speed //time between the end of one operation to the start of another operation

  if (digitalRead(3) == 1): //operation of micro switch (Normally Open) to switch ON/OFF of the Arduino Water Wave Generator
    delay(50);
    current = 1; //the system can be stopped/resumed by pressing the micro switch
  }
  else current = 0;
  previous = sq(previous - current); //LOGIC equation to enable the sequence of (ON-OFF-ON-OFF...)for Arduino Water Wave Generator

  if (previous == 0) {
    Serial.print("run ");Serial.println(delaytime);
    myservoleft.write(165); //tell left servo motor arm to go to position in variable, '165 degree angular displacement'
    myservoright.write(165); //tell right servo motor arm to go to position in variable, '165 degree angular displacement'
    delay(delaytime); //waits 690 ms for the servo motors to start the subsequent operation, 'to move to 0 degree'

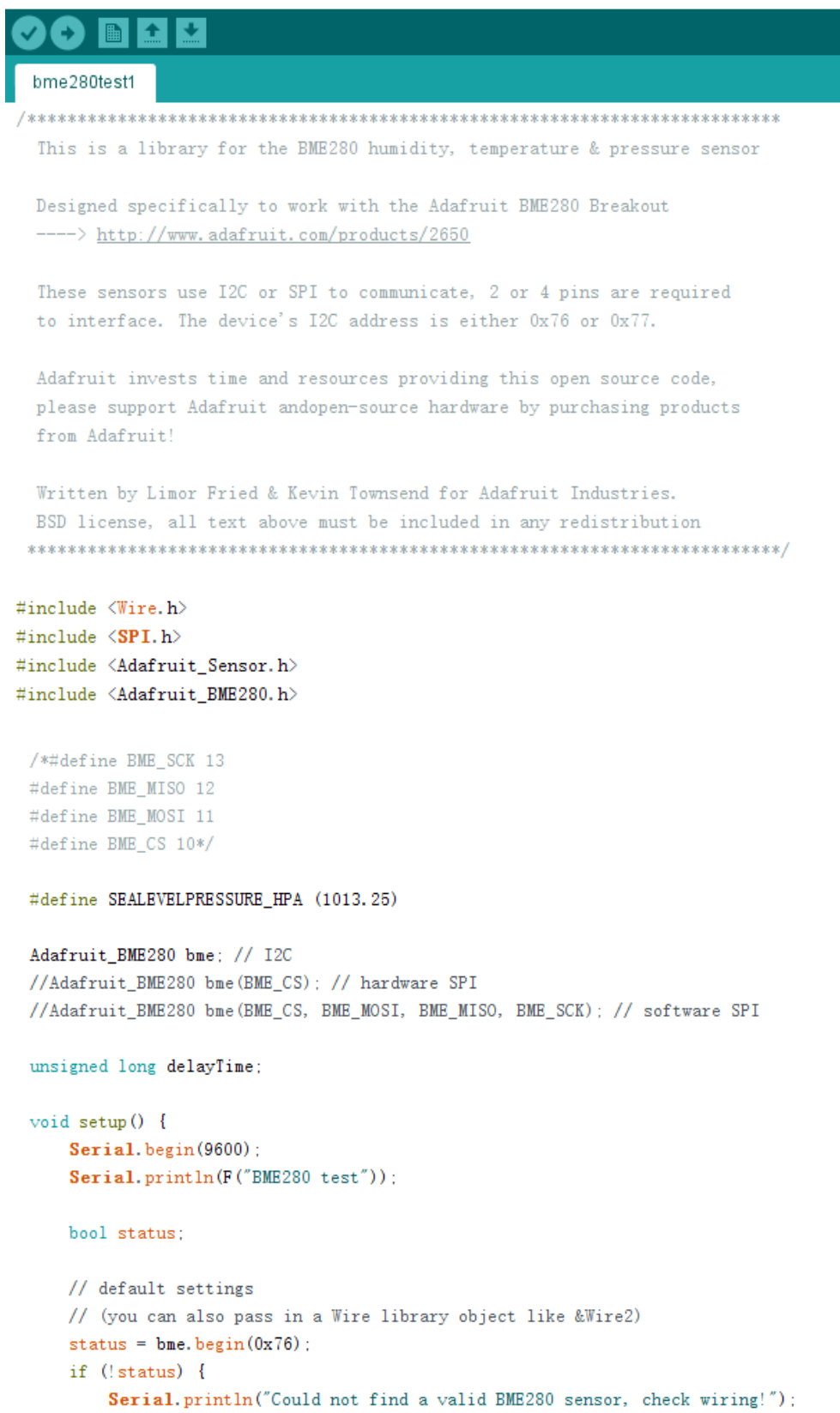
    myservoleft.write(0); //tell left servo motor arm to go to position in variable, '0 degree angular displacement'
    myservoright.write(0); //tell right servo motor arm to go to position in variable, '0 degree angular displacement'
    delay(delaytime); //waits 690 ms for the servo motors to start subsequent operation, 'to move to 165 degree'
  }
  else {
    Serial.println("stop"); //tell the servo motors to stop
    delay(3000);
  }
}
}

Done Saving.

```

APPENDIX H: Coding of the Pressure Sensor

The coding is edited from (Fried and Townsend, 2019).



```

bme280test1
/*****
  This is a library for the BME280 humidity, temperature & pressure sensor

  Designed specifically to work with the Adafruit BME280 Breakout
  ----> http://www.adafruit.com/products/2650

  These sensors use I2C or SPI to communicate, 2 or 4 pins are required
  to interface. The device's I2C address is either 0x76 or 0x77.

  Adafruit invests time and resources providing this open source code,
  please support Adafruit andopen-source hardware by purchasing products
  from Adafruit!

  Written by Limor Fried & Kevin Townsend for Adafruit Industries.
  BSD license, all text above must be included in any redistribution
  *****/

#include <Wire.h>
#include <SPI.h>
#include <Adafruit_Sensor.h>
#include <Adafruit_BME280.h>

/*#define BME_SCK 13
#define BME_MISO 12
#define BME_MOSI 11
#define BME_CS 10*/

#define SEALEVELPRESSURE_HPA (1013.25)

Adafruit_BME280 bme; // I2C
//Adafruit_BME280 bme(BME_CS); // hardware SPI
//Adafruit_BME280 bme(BME_CS, BME_MOSI, BME_MISO, BME_SCK); // software SPI

unsigned long delayTime;

void setup() {
  Serial.begin(9600);
  Serial.println(F("BME280 test"));

  bool status;

  // default settings
  // (you can also pass in a Wire library object like &Wire2)
  status = bme.begin(0x76);
  if (!status) {
    Serial.println("Could not find a valid BME280 sensor, check wiring!");
  }
}

```

```
    while (1);
}

Serial.println("-- Default Test --");
delayTime = 1000;

Serial.println();
}

void loop() {
    printValues();
    delay(delayTime);
}

void printValues() {
    Serial.print("Temperature = ");
    Serial.print(bme.readTemperature());
    Serial.println(" *C");

    Serial.print("Pressure = ");

    Serial.print(bme.readPressure() / 100.0F);

    Serial.println(" hPa");

    Serial.print("Approx. Altitude = ");
    Serial.print(bme.readAltitude(SEALEVELPRESSURE_HPA));
    Serial.println(" m");

    Serial.print("Humidity = ");
    Serial.print(bme.readHumidity());
    Serial.println(" %");

    Serial.println();
}
```
